Compressibility of the two-dimensional electron gas: Measurements of the zero-field exchange energy and fractional quantum Hall gap

J. P. Eisenstein, L. N. Pfeiffer, and K. W. West
AT&T Bell Laboratories, Murray Hill, New Jersey 07974
(Received 22 December 1993)

A quantitative study of the compressibility of the two-dimensional electron gas in GaAs heterostrutures is reported. Using a recently developed capacitive technique that avoids the large offset signals characteristic of conventional methods, high-precision compressibility data at both zero and high magnetic field has been obtained. The curious *negative* sign of the compressibility in certain regimes is shown to be a consequence of electron-electron interactions. Detailed numerical calculations show that the zero-field data are fully consistent with the known exchange energy, provided the finite thickness of the electron gas is properly included. At high magnetic fields, in the extreme quantum limit, the integrated compressibility signal is used to obtain a quantitative measure of the chemical potential discontinuity associated with the $\nu=\frac{1}{3}$ fractional quantum Hall effect. Comparison with a theoretical model which includes quasiparticle interactions has allowed a determination of the inhomogeneous broadening due to density fluctuations and has provided evidence of a second, apparently distinct, source of disorder. While the origin of this disorder is not fully understood, the data are consistent with simple lifetime broadening of the quasiparticle states.

I. INTRODUCTION

One of the central aspects our present understanding of the fractional quantum Hall (FQHE) effect found in two-dimensional electron systems (2DES) is the anticipated incompressibility of the underlying quantum liquid ground state.[1] While more than a decade has passed since the discovery[2] of the FQHE, the great majority of reported experimental findings are the result of electrical transport measurements or, in a growing number of cases, optical studies. Observing incompressibility, or the lack of it, requires a thermodynamics experiment and there have been very few of these, even in the integer QHE regime. The reason for this is simply the small number of electrons to be measured and often the presence of large unwanted background signals. Nevertheless, thermodynamic measurements provide information about the 2DES not readily obtained from transport studies where the distinction between localized and extended electronic states is critical. For example, several thermodynamic measurements, including specific heat,[3,4] magnetization,[5,6] and magnetocapacitance,[7–9] have demonstrated the existence of substantial numbers of localized states in the gaps between disorder-broadened Landau levels. These nonconducting states are not directly detectable in transport studies. Similarly, in the FQHE regime, despite the impressive convergence between the measured[10] transport mobility gap and the theoretically predicted[11] quasiparticle gap that has developed over the last few years, we can expect thermodynamics experiments to reveal localized quasiparticle states within the gap. One consequence of these localized states will be a suppression of incompressibility.

In an earlier publication[12] we reported qualitative results from a study of the thermodynamic compressibility K of the 2DES at both zero and high magnetic field. The compressibility K is simply related to the total energy $E_{\rm tot}$ (per unit area), chemical potential μ, and areal density N of the system:

$$K^{-1}=N^2\frac{\partial^2 E_{\rm tot}}{\partial N^2}=N^2\frac{\partial\mu}{\partial N}\ . \tag{1}$$

These relations illustrate the close connection of the compressibility to the underlying equation of state,[13] a quantity of fundamental importance and one generally more amenable to theoretical analysis than the transport or optical response of the system. The advantage of a highly sensitive and selective, capacitive technique[12] and the availability of high-quality samples allowed us to easily detect the thermodynamic signatures of electron-electron interactions in the 2DES, not only in the fractional quantum Hall regime,[14] but also at zero magnetic field where, to our knowledge, prior results did not exist. These results highlighted the advantages of thermodynamic probes of the 2DES by revealing qualitative aspects of the system not apparent in transport measurements. Prominent among these was the finding that the compressibility of the 2DES can become *negative,* owing to interactions, at low enough densities.[13,15] At zero magnetic field this effect is due primarily to the exchange energy while at high field[16,17] the correlation energy plays a significant role as well. An additional qualitative result was the observation of deep minima straddling the compressibility peaks at the $\nu=\frac{1}{3}$ and $\frac{2}{3}$ FQHE states. These minima were interpreted[12,18] as strong evidence for the existence of the interacting quasiparticle gases central to the theory of the FQHE.

In this paper, beyond elaborating on these earlier findings, we present the results of a quantitative study of the observed compressibility features. The plan of the paper is as follows. Section II is devoted to experimental

issues. Included is a description of the technique we have developed for measuring $\partial\mu/\partial N$, a discussion of how the raw data is prepared for analysis and, finally, a brief account of how the samples are grown and processed. In Sec. III we demonstrate that compressibility measurements at zero magnetic field allow a quantitative determination of the exchange energy, so long as the finite thickness of the 2DES is properly accounted for. Section IV covers the high-field results, concentrating on the fractional quantum Hall regime. The strong compressibility signatures at the $\nu=\frac{1}{3}$ FQHE state are used to obtain values for the chemical potential discontinuity associated with this curious quantum liquid. Comparison of the results with theory gives a quantitative measure of the disorder in the sample and suggests that beyond simple inhomogeneous broadening due to density fluctuations a second, independent, gap suppression mechanism exists. In Sec. V we summarize our findings and conclude the paper with remarks about possible future directions.

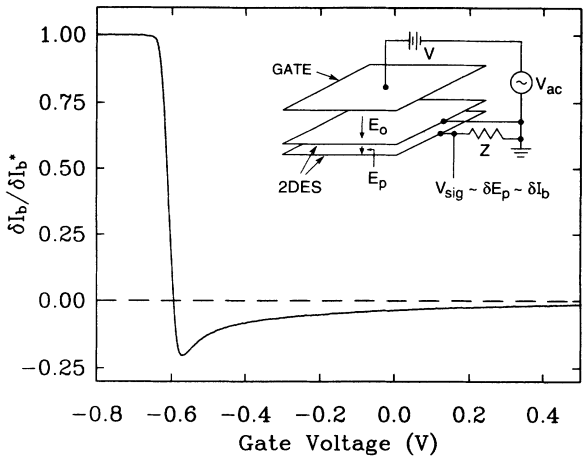

FIG. 1. Current flow onto lower 2DES layer vs dc gate voltage at $T=0.3$ K and zero magnetic field. This current is directly proportional to the differential penetrating electric field δE_p. The data are normalized by $\delta I_b^*=1.59$ nA, the current measured with the top 2DES depleted. Inset: Schematic depiction of experimental arrangement.

II. EXPERIMENTAL METHOD

A. Field penetration technique

The method employed here to determine the compressibility of the 2DES is an improvement on a standard capacitive one.[19] In the conventional scheme the capacitance between the 2D gas and a metal gate electrode is measured. This capacitance is of course largely determined by the distance between the gate and the 2DES and the dielectric properties of the intervening insulating layer, but it also depends upon the density of states, or compressibility, of the 2DES itself. The dominance of a large geometric term in the measured capacitance essentially forces one to vary some other parameter, like magnetic field, and then subtract off a large, and hopefully constant, offset in order to uncover the 2D contribution. This approach has been widely used to assess the Landau-level density of states for 2D systems.[7–9] There are two major drawbacks to this technique. First, the geometric term is usually not accurately known and therefore the subtraction is uncertain. At zero magnetic field this difficulty leaves even the *sign* of the 2D compressibility unknown. The geometric term produces a second difficulty as well: it may not actually remain constant as the external parameter is changed. For example, measuring the dependence of the 2D compressibility upon sheet density usually requires application of dc potentials to the gate electrode in addition to the small ac voltage used to measure the capacitance. The resulting large dc electric field can alter the dielectric properties of the spacer region between the gate and the 2D gas, and thus change the magnitude of the geometric capacitance. This leaves the subtraction procedure problematic. This problem can be significant in modulation-doped GaAs heterostructures where Si dopant layers often lie in the spacer region between the gate and the 2DES.

The present capacitive technique avoids these problems by, in effect, automatically subtracting the geometric term. This is achieved by use of a double layer 2D system and measuring the fraction of the ac electric field δE_0 applied by the gate which penetrates one layer and impinges upon the second. The inset to Fig. 1 contains a schematic diagram of the basic configuration. As the diagram shows, the "top" 2D layer of the pair is grounded. Assuming there is no direct stray capacitance between the gate and the bottom 2DES, any ac electric field terminating on the bottom layer will have penetrated the top layer. Such an ac penetration field δE_p will require current flow across the external impedance Z and thus will generate a detectable voltage $V_{\rm sig}$. It is intuitively clear that any nonzero δE_p exists only because of the finite screening ability, or compressibility, of the top 2D layer. Thus the entire observed signal voltage reflects the compressibility of the top layer; there is *no* offset. Figure 1 also contains a typical scan of the ac current flowing onto the lower 2DES due to the penetration of an applied ac gate electric field through the grounded upper 2DES. This signal is plotted versus the dc component of the gate voltage used to provide a sweep of the average density of the upper 2DES. The observed *negative* sign of the penetration signal, one of the central findings of this work, reflects the substantial impact of Coulomb interactions on the thermodynamics of typical 2DES's in GaAs.

In order that the measured currents flowing on and off the lower layer accurately reflect the thermodynamic properties of the upper 2DES, it is essential to keep the measurement frequency low enough that the finite conductivities of the two electron gases do not play any role. If the conductivity is too low (a question of RC time constants) then the field penetration will be enhanced above its thermodynamic value. At zero magnetic field the high mobility of the 2DES's allows measurements in the kHz range without producing significant quadrature signals or affecting the capacitive component. At high magnetic field, however, problems can arise, especially if either 2DES enters a quantum Hall state where its conductivity σ_{xx} vanishes exponentially at low temperature. Careful

examination of the frequency and temperature dependences of both phases of the observed signal voltage was required to establish acceptable ranges for these parameters. As a result, spurious conductivity effects do not contribute to the bulk of the data presented here. The only situations in which such nonequilibrium effects could not be entirely eliminated was when the upper 2DES was very near to complete depletion or extremely close to strong *integer* quantum Hall states. None of our conclusions are affected by these cases.

To extract quantitative information about the 2D compressibility from the observed penetration signal requires consideration of several effects. Important among these are two that stem from the finite thickness of the 2D layers themselves: a softening of the Coulomb repulsion between electrons and bending of the conduction-band edge in the quantum wells. While both of these will be addressed in detail below, we give here simple results for the idealized case of two infinitely narrow quantum wells separated by a distance s_2 with a gate electrode deposited a distance s_1 above the top 2DES. This geometry is schematically illustrated in Fig. 2(a). Let the gate be biased to a voltage V with respect to the common chemical potential of the two 2D layers which we assume to be in equilibrium with each other. A small change δV in the gate voltage will produce a change δE_0 in the electric field between the gate and the top 2DES and δE_p in the electric field between the two layers. (We assume that there is no change in the electric field beneath the bottom layer; this is equivalent to assuming that there are no additional parallel conducting layers in equilibrium with the bilayer 2DES. We also assume that the layer spacing is large enough that any *interlayer* many-body effects[20] can be ignored.) Let $\delta\mu_{t,b}$ be the resultant changes in the chemical potentials of the two 2DES's (measured relative to the bottoms of the respective quantum wells) and $\delta N_{t,b}$ the associated changes in the two sheet densities. We have (in the SI units used throughout this paper)

$$e\delta V = es_1\delta E_0 + \delta\mu_t \ , \qquad \delta\mu_t = \delta\mu_b + es_2\delta E_p \ , \tag{2}$$

and, from Gauss's law,

$$\delta E_0 = (e/\varepsilon)(\delta N_t + \delta N_b) \ , \qquad \delta E_p = (e/\varepsilon)\delta N_b \ . \tag{3}$$

Combining these relations we arrive at

$$\delta V = \delta E_0[s_1 + d_t(d_b + s_2)/(d_t + d_b + s_2)] \tag{4}$$

and, most importantly,

$$\delta E_p/\delta E_0 = d_t/(d_b + d_t + s_2) \ , \tag{5}$$

where we have defined the fundamental distance parameters:

$$d_{t,b} \equiv (\varepsilon/e^2)(\partial\mu/\partial N)_{t,b} \ . \tag{6}$$

Equation (5) expresses the basic advantage of the present experimental approach: measuring the penetrating electric field δE_p, which is proportional to the current flowing onto the bottom 2DES, provides direct access to $\partial\mu/\partial N$ for the top 2DES without any offset signals. From Eq. (1) we see that this constitutes a direct measure of the compressibility K of the top 2DES. Note that Eq. (5) shows that the penetration also depends on the compressibility of the bottom 2DES. Usually, however, the penetration is fairly weak ($s_2 \gg d_t$ and d_b) and the bottom layer density remains close to its nominal value for all dc gate voltages until the top layer depletes. Indeed, for noninteracting 2D electrons $d_t = d_b = \pi\varepsilon\hbar^2/m^*e^2 = a_0/4$, with a_0 the semiconductor Bohr radius. In GaAs $a_0/4 \approx 25$ Å and since the quantum well spacing s_2 is several hundred Å, the typical penetration would be only a few percent, and would be positive.[21] As we have shown,[12] this result is qualitatively altered by electron-electron interactions, with the observed differential penetration often being of opposite sign to the applied field.

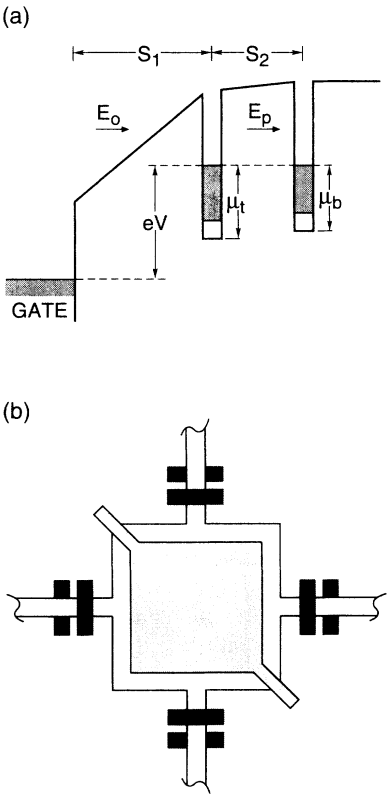

FIG. 2. (a) Simplified band diagram of the gated double quantum well structure. The shaded region in each quantum well denotes the Fermi distribution of the 2D electrons. The chemical potentials $\mu_{t,b}$ are measured relative to the bottoms of the individual wells. (b) Mesa and gate layout. The central mesa and gate squares are 250 and 210 μm, respectively, on a side. Each of the mesa arms is terminated with an indium Ohmic contact and has two associated gates, on the sample front and back sides, used for establishing separate connections to the individual 2D electron layers.

B. Data analysis

Experimentally it is the current δI_b flowing onto the lower layer in response to the ac gate excitation voltage

δV which is measured. This current is directly proportional to the ac penetrating electric field δE_p. To employ Eq. (5), however, we must also know the applied electric field δE_0. While this can be accomplished by simultaneously measuring the current flowing onto *both* 2D layers and then using Eq. (3) to determine the ratio $\delta E_p/\delta E_0$, we have chosen to employ a simpler, if slightly less accurate, method that requires only the lower layer current be measured. (In those instances where both methods have been compared, the difference in the deduced $\delta E_p/\delta E_0$ is completely negligible.) The simpler procedure relies on estimating δE_0 from the lower layer current measured when the upper layer is fully depleted (by a large negative dc gate bias), for then $\delta E_p=\delta E_0$. Prior to depletion, of course, the actual δE_0 value is larger by roughly the factor $1+s_2/s_1\sim 1.07$ and depends on the penetration itself. Defining δE_0^* as the applied electric field when the top 2DES is depleted ($d_t\rightarrow\infty$), using Eq. (4) gives

$$\delta E_p/\delta E_0=\frac{\delta E_p/\delta E_0^*}{[1+\gamma(1-\delta E_p/\delta E_0^*)]}\ , \tag{7}$$

where $\gamma=(d_b+s_2)/s_1\sim 0.07$. Equation (7) provides $\delta E_p/\delta E_0$ solely in terms of the measured bottom layer current δI_b, since

$$\delta E_p/\delta E_0^*=\delta I_b/\delta I_b^* \tag{8}$$

with δI_b^* the current measured with the top layer depleted. While Eq. (7) does depend on the validity of the narrow well approximation, it does so only very slightly. In essence, this equation merely corrects the estimate of the applied field δE_0 for the different distances between the gate and the two 2DES's. Since this correction is only about 7% in our samples, any additional error incurred by neglecting the thickness of the quantum wells can be safely ignored. The truly important consequences of the finite thicknesses appear in the measured δE_p, *not* in the estimated δE_0.

Finally, since it is the dependence of the compressibility on sheet density that is desired, a conversion algorithm between dc gate voltage and top 2DES density must be established. Determination of the nearly linear proportionality between these two quantities is greatly simplified by the observation of signatures in the penetration signal in an applied magnetic field that can be unambiguously associated with specific Landau-level filling fractions. On the other hand, the exact relation depends upon the penetrating field itself. This can create significant nonlinearities when the penetration is strong, irrespective of its sign. To account for this, we use Eqs. (3), (4), (7), and (8) to relate the ratio $\delta N_t/\delta V$ to the differential penetration $\delta E_p/\delta E_0^*$ and normalized lower layer current $\delta I_b/\delta I_b^*$:

$$\delta N_t/\delta V=\frac{\varepsilon}{es_1}\beta(1-\delta E_p/\delta E_0^*)=\frac{\varepsilon}{es_1}\beta(1-\delta I_b/\delta I_b^*)\ . \tag{9}$$

This equation is then numerically integrated to determine $N_t(V)$. The factor β, typically around 0.9, has been inserted to adjust this relation to fit the known features observed in an applied magnetic field. Given the uncertainties in the dielectric properties of the doped semiconductor layers between the double quantum wells (DQW) and the gate and the simple narrow-well model used to derive Eq. (9), this $\sim 10\%$ correction seems reasonable. A minor complication with this scheme concerns the appropriate endpoints for the integral of Eq. (9). In particular, to establish the gate voltage at which the density $N_t=0$ would require the integration to span the region where the upper 2DES is depleting. This is problematic, however, since extremely close to depletion the observed penetration eventually must become polluted by the vanishing sheet conductivity. This problem is dealt with by integrating Eq. (9) across depletion but adding on a constant of integration $N_{\rm off}$. This offset, along with the parameter β, is then adjusted to give a best fit to the density fixed points observed in a magnetic field. While the typical β values are around 0.9, the accompanying density offsets are typically only $N_{\rm off}\sim 2.0\times 10^9$ cm^{-2}, about 2.5% of the nominal ungated density of either 2D layer. The constant $N_{\rm off}$ sets a lower limit on the density at which we can draw conclusions about the 2DES compressibility.

In the foregoing discussion we have largely ignored the effect of the lower layer compressibility, which enters via the parameter d_b, assuming it has little quantitative impact. This is almost always an excellent assumption, provided the lower layer does not enter a quantum Hall state. Not only is d_b numerically much smaller than s_2, the quantum well center-to-center spacing, but, since the penetration effect itself is small, the density N_b of the lower layer remains close to its nominal value. At zero magnetic field, in fact, the net change in N_b over the entire range of gate voltage (before depletion of the upper layer) is only about 10%. Consequently, our approach has been to simply replace d_b by a constant which is readily determined from applying Eq. (5) to the observed penetration at zero gate bias where, since the DQW is then well balanced, we can assume $d_b=d_t$. It is completely adequate to use the uncorrected penetration, $\delta E_p/\delta E_0^*$, for this determination.

C. Samples and processing

The double layer 2D systems employed in this work are standard GaAs/Al_xGa_{1-x}As double quantum wells (DQW) grown by molecular-beam epitaxy (MBE) on ⟨100⟩-oriented GaAs semi-insulating substrates. While a number of samples with varying structures have been grown and studied, specific parameters will be given here only for the one used in the present quantitative work. The compressibility data from this sample show that its upper 2DES is less disordered than that in any similar sample yet examined. The DQW consists of two 200-Å-wide GaAs quantum wells separated by an undoped 175-Å $Al_{0.33}Ga_{0.67}As$ barrier. The well center-to-center distance is thus $s_2=375$ Å. The barrier is sufficiently thick that tunneling, while detectable, is so weak that it plays no role in these experiments. The DQW is embedded in thick $Al_{0.33}Ga_{0.67}As$ cladding layers. The total distance between the sample top surface and the center of the top

GaAs well is $s_1 = 5300$ Å. The lower GaAs well is populated with electrons donated by a Si δ layer 1650 Å below it in the alloy cladding layer while a similar Si layer is deposited 1400 Å above the upper GaAs well. This doping configuration[22] results in high-mobility 2D gases with about 7.5×10^{10} cm^{-2} carriers in the lowest subband of each quantum well. Standard magnetotransport measurements on the individual 2DES's yield mobilities of 2.1 and 0.6×10^6 cm^2/Vs for the upper and lower layers. Several fractional quantum Hall states are readily detected in the transport at high magnetic fields.

The basic measurement geometry is illustrated in Fig. 2(b). A square mesa, 250 μm on a side, is created using standard photolithographic techniques. Four 20-μm-wide arms extend from the sides of the mesa. Each is eventually terminated with a diffused In Ohmic contact. The gate electrode used to form a capacitor is deposited onto the sample front surface. Note that this gate (210×210 μm) does not overlap the mesa edge except where thin contact arms extend out and away from the central mesa. This was done in order to reduce the direct stray capacitance between the gate and the lower 2DES occurring where the gate metal overlaps the mesa edge. This stray capacitance, though small, adds a positive offset to the apparent $\delta E_p/\delta E_0$ values. The nonoverlapping gate geometry has reduced this capacitance by a factor of about 12 relative to our earlier measurements.[12] This stray capacitance is estimated to not exceed 0.05 pF. This value is comparable to the fluctuations in the baseline differential penetration at zero gate bias observed from one sample cooldown to the next.

As Fig. 2(b) shows, each of the arms extending out from the central mesa is crossed by two additional gates, one on top the sample and the other underneath the DQW on the sample backside. These gates are used to establish the separate electrical connections to the individual 2D layers essential to the entire technique. As detailed elsewhere[23] any of these gates can be biased so as to locally completely deplete the nearer 2DES without seriously affecting the remote layer. In this way an Ohmic contact at the end of any arm is connected to the central mesa through only one of the 2D layers. In practice, for these experiments two of the arms are completely "cut off" by biasing the two appropriate top gates strongly enough to deplete *both* of the underlying 2DES's. For the remaining two contact arms, one is rendered a top layer contact by biasing the associated backside gate till the lower 2DES is locally depleted, while the other is made a bottom layer contact by biasing the relevant top gate. (In order that the required back gate biases are not too large, and reasonable lateral definition of the gated region is maintained, the sample is thinned to a total thickness of around 50 μm before the backside gates are deposited.)

III. ZERO MAGNETIC FIELD

A. Experimental results

Figure 1 shows the detected ac current δI_b at zero magnetic field flowing onto the lower 2DES in response to an ac gate excitation of 20 mV at 2 kHz. The data have been normalized, as discussed above, by the current δI_b^* measured when the upper 2DES is fully depleted. The dc component of the gate voltage V is swept from +0.5V down to −0.8V, reducing the upper 2DES density N_t from a maximum of about 1.3×10^{11} cm^{-2} down to zero at $V\approx-0.6$ V. These data were taken at a temperature of $T=0.3$ K, but no significant changes were observed up to about $T=2$ K, except very close to depletion. As the figure shows, the sign of the differential penetration field δE_p ($\propto\delta I_b$) is *negative* over the entire range of gate voltage except near depletion where an increasing fraction of the applied electric field δE_0 begins to penetrate. Immediately prior to depletion the data suggest an incipient negative *divergence* in $\partial\mu/\partial N$ for the upper 2DES.

To convert between dc gate voltage and sheet density the differential penetration field is measured with a small magnetic field B applied perpendicular to the 2D planes. Figure 3 contains data obtained at $B=0.2$ T. The oscillations observed at this magnetic field reflect the modulation of the 2D density of states $\partial N/\partial\mu$ due to the formation of Landau levels. At each local maximum the Fermi level of the upper 2DES is centered in the gap between two Landau levels. At this low magnetic field the spin Zeeman splitting of the levels is not resolved. Thus, on moving from one maximum to the next the density in the upper 2DES changes by $\Delta N_t = 2eB/h$ and the filling factor $\nu_t \equiv hN_t/eB$ by $\Delta\nu_t = 2$. Furthermore, by observing the magnetic-field dependence of the oscillation pattern, it is possible to assign a precise value of ν, and hence density, to each maximum in the penetration signal. The solid dots in Fig. 3 show this determination.

As outlined earlier, the variation of N_t with gate voltage depends on the differential penetration itself and Eq.

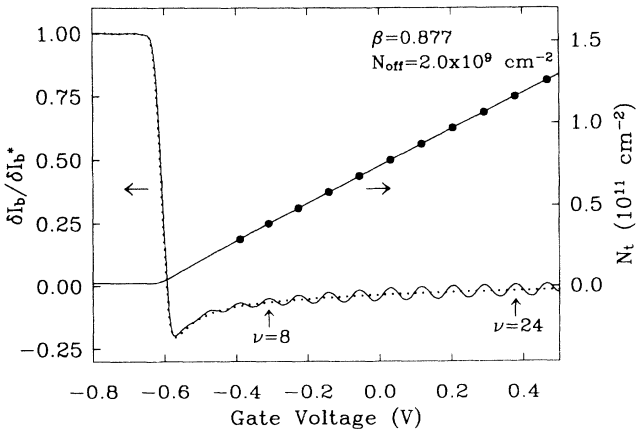

FIG. 3. Density calibration. The solid oscillating curve shows the uncorrected differential penetration in a $B=0.2$ T magnetic field. (The lightly dotted curve shows the zero-field data.) Each peak corresponds to a specific filling fraction ν_t and therefore density $N_t = \nu_t eB/h$; these are represented by the solid dots. The diagonal solid curve is the final density-gate voltage calibration obtained after integrating Eq. (9), with the zero-field data inserted, and adjusting the parameters β and $N_{\rm off}$ for a best fit to the solid dots.

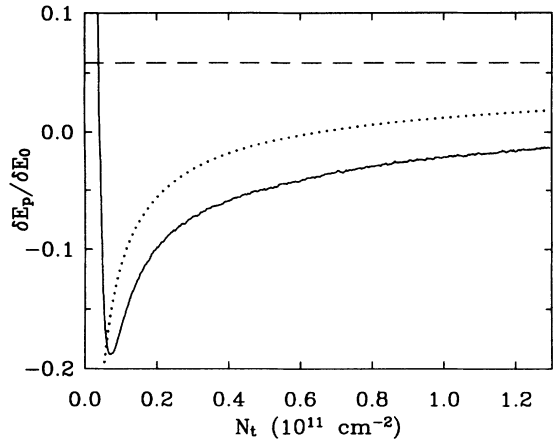

FIG. 4. Differential penetration vs upper 2DES density at $T=0.3$ K and zero magnetic field. The horizontal dashed line assumes noninteracting electrons; the dotted curve includes the exchange energy but omits all finite thickness effects.

(9) expresses this dependence. The solid line in Fig. 3 results from integrating Eq. (9) (with the zero field $\delta I_b/\delta I_b^*$ data shown in Fig. 1 inserted) and adjusting the parameters β and $N_{\rm off}$ for a best fit to the set of densities determined from the Landau-level analysis of the $B=0.2$ T data. With $s_1=5300$ Å and $\varepsilon=11.0\varepsilon_0$ (appropriate[24] to the $Al_{0.33}Ga_{0.67}As$ alloy layer above the DQW), a least-squares fit gives $\beta=0.877$ and $N_{\rm off}=2.0\times10^9$ cm^{-2}.

The final step in the data reduction consists of using Eqs. (7) and (8) to make the small ($\sim7\%$) correction to the estimated applied gate field δE_0. To apply these equations we need to estimate d_b, the parameter reflecting the lower layer compressibility. As mentioned above, this is done by simply applying Eq. (5) to the measured $\delta E_p/\delta E_0^*$ value obtained at zero gate bias where the two 2DES's have nearly the same densities. As expected, the resulting estimate, $d_b\approx-12$ Å, has a negligible impact since it is so greatly exceeded by the quantum well center-to-center spacing $s_2=375$ Å and distance to the top gate $s_1=5300$ Å. Figure 4 contains the final plot of the fractional differential penetration $\delta E_p/\delta E_0$ versus top layer density N_t.

B. Analysis and discussion

The qualitative origin of the observed negative differential penetration field, and thus the negative $\partial\mu/\partial N$ for the upper 2DES, lies in the dominance, at low density, of Coulomb interactions over kinetic effects. For a noninteracting infinitely thin 2DES $\partial\mu/\partial N$ is a positive constant, independent of density. As mentioned in Sec. II, for GaAs under these assumptions, $d_t=d_b=a_0/4\equiv d_0\approx25$ Å. With $s_2=375$ Å, the quantum well center-to-center spacing, the expected differential penetration would be, using Eq. (5), $\delta E_p/\delta E_0=1/(2+s_2/d_0)=0.059$. The dashed line in Fig. 4 shows that this simple estimate is completely wrong. On the other hand, including electron-electron interactions, even at the lowest level, lays bare the origin of the negative compressibility. For this model of the ideally thin 2DES, the total energy per unit area is, in Hartree-Fock approximation,

$$E_{\rm tot}^{\rm HF}=(\tfrac{1}{2}\varepsilon_F+\varepsilon_{\rm ex})N\ , \tag{10}$$

where N is the sheet density, $\varepsilon_F=N\pi\hbar^2/m^*$ the Fermi energy, and $\varepsilon_{\rm ex}$ the exchange energy per electron. (For now we are ignoring any contributions to the energy arising from the confinement of the 2DES in the quantum well.) In this ideal 2D model the exchange energy is given by[25]

$$\varepsilon_{\rm ex}=-\frac{4}{3}(2/\pi)^{1/2}\frac{e^2}{4\pi\varepsilon}N^{1/2}\ . \tag{11}$$

Using Eq. (1) allows the calculation of $\partial\mu/\partial N$:

$$\frac{\partial\mu}{\partial N}=\frac{e^2d_0}{\varepsilon}[1-(N_c/N)^{1/2}] \tag{12}$$

with the critical density $N_c=(8\pi^3d_0^2)^{-1}\approx6.5\times10^{10}$ cm^{-2}. While at very high density $\partial\mu/\partial N$ approaches the noninteracting result, as N is reduced it deviates more and more, becoming negative for $N<N_c$. As $N\to0$ Eq. (12) predicts that $\partial\mu/\partial N$ diverges negatively, as $N^{-1/2}$. Again employing Eq. (5) (with the lower layer density set to $N_b=7.5\times10^{10}$ cm^{-2}) leads to the dotted curve in Fig. 4. Unlike the noninteracting result, the figure shows that Eq. (12) captures the essential physics underlying the experimentally observed differential penetration.

It is worth noting that the interaction-induced divergence in $\partial\mu/\partial N$ is truncated, by disorder presumably, at a density of only 7×10^9 cm^{-2}. This is very low by the standards of GaAs heterostructures. Using the conventional parameter $r_s\equiv a_0^{-1}(\pi N)^{-1/2}$, this density corresponds to $r_s\approx6.8$. (We emphasize that the effects of finite sheet conductivity do not become significant until still lower densities, comparable to $N_{\rm off}=2\times10^9$ cm^{-2}, are reached.) The truncation of $\partial\mu/\partial N$ implies, crudely, that the electron-electron interaction has become weaker than the disorder potential $V_{\rm dirt}$. From Eq. (11) then, we estimate $V_{\rm dirt}\sim1.0$ meV.

A system with negative thermodynamic compressibility is generally unstable. This does not apply, however, in the present case because the measured differential penetration field reflects only that portion of the total compressibility due to the 2DES itself. In Eqs. (10)–(12) the spatial separation between the 2DES and its associated positive neutralizing background (in the donor layers and on the gate electrode) has been ignored. The long-range electric fields due to these separations produce large capacitive contributions to the total energy which render the total compressibility positive. In fact, the main advantage of the present experimental technique lies in its discrimination against these long-range electric fields. Nevertheless, interesting stability questions can arise in situations closely related to the present one. For example, it has been suggested[26] that in a closely spaced DQW all the electrons will jump into one of the wells if the density is low enough, simply because the negative $\partial\mu/\partial N$ arising from exchange will eventually dominate the capacitive term. In addition to such global instabili-

ties, the negative compressibility might also create in-plane inhomogeneities, such as charge-density waves.

While the exchange contribution to the total energy is the essential reason that the observed 2DES compressibility becomes negative at low density, it is clear from Fig. 4 that other quantitative effects are at work as well. For example, consider the many-body corrections that go beyond Hartree-Fock approximation to include the effects of electron-electron *correlation*. Tanatar and Ceperley's[27] extensive Monte-Carlo calculations of the ground-state properties of the ideal 2DES at zero magnetic field show, however, that for the range of densities examined here the effect of correlation on the compressibility is not very large (~ 10–$20\,\%$ relative to the noninteracting case). A much more significant, if less fundamental, class of corrections to our experimental results stems from the finite thickness of the quantum wells. These include effects of the softened Coulomb repulsion between electrons and the Stark-like shifts of the quantum well confinement energies which accompany changes in density (or gate voltage). We begin by considering the Coulomb softening only. In Hartree-Fock approximation, Stern[28] described how to calculate the exchange energy including the extent of the electronic wave function in the z direction. In terms of the quantitity $r_s = a_0^{-1}(\pi N)^{-1/2}$, the "thickened" exchange energy is

$$\varepsilon_{ex} = -\frac{8\sqrt{2}}{3\pi}\left[\frac{e^2}{8\pi\varepsilon a_0}\right] r_s^{-1} F(r_s,\phi(z)) \ . \tag{13}$$

This result is identical to Eq. (11), aside from the form factor $F(r_s,\phi(z))$ which depends upon the shape of the electronic wave function $\phi(z)$. To evaluate the form factor F we have made the simplifying assumption that $\phi(z)$ is adequately approximated by the ground-state wave function of an infinite square well of width w. Borrowing an integral from Price,[29] we have numerically evaluated the function F which, in this case, depends on the single variable $\zeta = w/a_0 r_s$. Once $F(\zeta)$ is known Eqs. (1), (10), and (13) are employed to determine $\partial\mu/\partial N$. (The details are given in the Appendix.) Since the finite thickness reduces the magnitude of the exchange energy it can only *lessen* the tendency toward negative compressibility and this, as Fig. 4 proves, will merely worsen the agreement between theory and experiment.[30]

In order to completely account for the finite thicknesses we have to include contributions to the total energy E_{tot} coming from the confinement of the 2DES in the quantum well. If the subband energies in the well were independent of electron density N, the increment to E_{tot} would be linear in N and would therefore not affect $\partial\mu/\partial N$ $(=\partial^2 E_{tot}/\partial N^2)$. This is, unfortunately, not a good approximation here and the distortions of the potential wells owing to the space charge of the electrons are significant. With the subband energies depending upon electron density, a nonzero effect on $\partial\mu/\partial N$ results. To assess these band-bending effects we have self-consistently solved the Schrödinger and Poisson equations for the double quantum well system;[31] the details of these numerical procedures are left to the Appendix. As will become evident, this has led to quantitative agreement with the experimental results.

The inclusion of these Hartree band-bending effects makes a *negative* contribution to the differential penetration field. When electrons are added to the upper quantum well, by positively incrementing the gate bias voltage, the induced electric field pulls the 2DES toward the upper interface of the well. This makes the potential more asymmetric, and causes the ground-state energy to fall *relative to the lower interface of the quantum well.* While if taken alone this would produce a negative $\partial\mu/\partial N$, it is offset by the positive contribution from the noninteracting density of states (i.e., d_0). In the absence of interaction effects we have found the net $\partial\mu/\partial N$ remains positive at all densities in our samples, at least at zero magnetic fields. We emphasize that these Hartree effects, while pushing $\partial\mu/\partial N$ more negative, are qualitatively distiguishable from the interaction effects. In particular, they are only weakly density dependent and lack the divergence in the limit $N \to 0$ that is characteristic of the many-body effects.[32]

The numerical approach we have taken is to self-consistently determine the electron density in each quantum well for a given distribution of the positive background charge. This background charge is assumed to lie in two sheets, one above and one below the DQW, each producing a uniform electric field. The action of the gate electrode is simulated by simply altering the positive background density above the DQW. Then, after arbitrarily dividing the total electron density (equal to the total background density) between the quantum wells, the ground subband energy and Fermi level in each well is separately determined by self-consistent solution of the Schrödinger and Poisson equations. If a mismatch of the Fermi levels exists, charge is transferred from one well to the other and the calculation is repeated. This process is iterated until convergence with matched Fermi levels is obtained. (Note that this does not generally imply a flat-band condition in the barrier layer.) The assumption that the wells can be treated independently is justified by the tiny magnitude ($< 10^{-4}$ meV) of the tunneling-induced splitting of the ground symmetric and antisymmetric states of the DQW when it contains equal densities in each well. Once the density in each well is determined for a large number of gate charge levels, the differential penetration $\delta E_p/\delta E_0$ is determined from the variation of the lower quantum well density N_b with the background charge on the gate N_g. After pairing these results with the calculated upper quantum well densities N_t comparison with experiment can be made.

Many-body effects have been incorporated into these calculations in either of two ways. The first approach treats interactions in a thickened 2D Hartree-Fock approximation. At each step in the interwell self-consistency loop, the subband energy ε_0 in each well is calculated in Hartree approximation, i.e., ignoring exchange. The chemical potentials are then determined by adding to ε_0 the appropriate Fermi energy ε_F and an exchange contribution μ_{ex}. The interwell loop is then allowed to proceed. The term μ_{ex} is calculated from Eq. (13) $[\mu_{ex} = \partial(N\varepsilon_{ex})/\partial N]$ with the simplifying assumption

that the form factor F remains adequately approximated using infinite square well wave functions. Consequently, this method does not treat the exchange fully self-consistently. We believe, however, that the errors incurred are small; this is supported by the near unit overlap (>98%) between the actual Schrödinger-Poisson wave functions and those of an infinite square well.

For our second method, we have employed the local-density approximation (LDA). In this approach exchange (and correlation) are treated three dimensionally by introducing an additional z-dependent term $v_{xc}(\phi(z))$ in the potential which depends upon the 2D subband wave function $\phi(z)$. This term is just the exchange-correlation contribution to the chemical potential of a fictitious homogeneous electron gas with 3D density $N|\phi(z)|^2$. Following Stern and Das Sarma,[33] we employ the Hedin-Lundqvist[34] functional for v_{xc}. With this term included in the potential, the calculated subband energies ε_0 include the many-body corrections. The chemical potential is then found by simply adding the Fermi energy: $\mu=\varepsilon_0+\varepsilon_F$. (We remark that if the correlation energy is omitted from the LDA functional, the calculated $\partial\mu/\partial N$ is only slightly changed over the density range appropriate here.)

Figure 5 compares these numerical results with the experiment. While both the experiment and the numerical results yield the differential penetration $\delta E_p/\delta E_0$, we have chosen to convert both into values for $d_t \propto \partial\mu_t/\partial N_t$ for the *equivalent* narrow-well structure. To do this the lower layer parameter d_b is first determined from the (measured or calculated) differential penetration obtained when the DQW is balanced by applying Eq. (5) with d_t set equal to d_b. Equation (5) is then inverted to obtain d_t at all densities. As Fig. 5 shows, the inclusion of both the Coulomb softening and the Hartree band bending into the calculations has produced good agreement with the data. The two different approaches for incorporating the many-body effects give results which the experiment cannot distinguish. The error bars attached to the thickened 2D Hartree-Fock results show the effect of a ±15% change in the exchange energy.

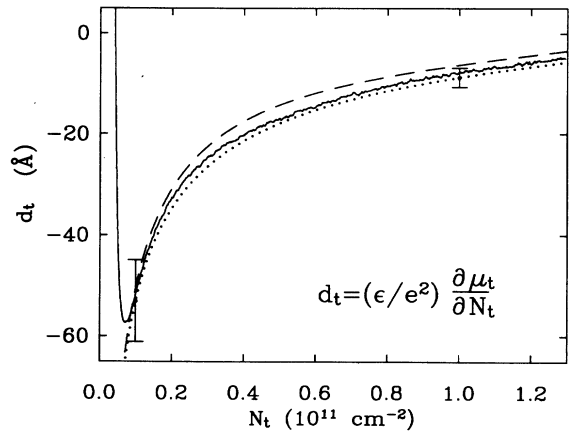

FIG. 5. Compressibility parameter d_t vs density from the zero magnetic-field data. Dashed and dotted curves are theoretical calculations in local-density approximation and thickened 2D exchange model, respectively. These calculations contain no adjustable parameters. The error bars on the dotted curve reflect ±15% changes in the exchange energy.

The most significant known sources of systematic error are the run-to-run fluctuations in the baseline differential penetration at zero gate bias, the small, but inevitable, direct stray capacitance between the gate and the lower 2DES, and the uncertainties in the density calibration. The run-to-run fluctuations and the (estimated) direct stray capacitance are of comparable magnitude, about 0.05 pF. This translates into shifts in d_t of only about 3 Å, roughly equal to the difference between the two numerical schemes used to incorporate the many-body effects. The uncertainty in the density calibration is important only very close to depletion where, as already mentioned, it is estimated not to exceed 2×10^9 cm^{-2}. As Fig. 5 shows, this does not noticeably degrade the agreement between theory and experiment.

These zero magnetic-field experiments serve to illustrate the power of the experimental technique employed here. At the qualitative level our data clearly reveal strong signatures of electron-electron interactions in the thermodynamic properties of typical 2D electron systems in GaAs. From detailed calculations we have shown that the experimental results are in good accord with our understanding of exchange effects in 2D systems, once various technical issues are addressed. The good agreement between theory and experiment found at zero magnetic field suggests that this experimental technique will be especially useful in situations where our understanding of the many-body physics is less developed. At high magnetic field, in the so-called "extreme quantum limit," where correlation effects dominate, this is very much the case and it is to this regime that we now turn.

IV. HIGH MAGNETIC FIELD

A. Experimental results: Qualitative

Figure 6(a) shows the normalized differential penetration field $\delta E_p/\delta E_0$ at $B=6$ T and $T=0.4$ K, the raw data having been reduced according to the scheme described in Sec. II. These, and almost all other high magnetic-field data, were obtained using a gate excitation voltage of 10 mV at 7 Hz. This frequency was found to be adequate, for $T\geq0.4$ K and $B\leq13$ T, to eliminate spurious signals arising from the finite 2DES conductivity σ_{xx}, except when the upper 2DES entered *integer* quantum Hall states or was very close to depletion. These experimental constraints were established by a careful examination of the frequency and temperature dependences of both signal phases when the upper layer was in the $\nu=\frac{1}{3}$ fractional quantum Hall state and σ_{xx} was therefore extremely small.

The gate voltage-to-density calibration procedure followed the method outlined in Sec. II. At magnetic fields above ~6 T, however, the Fermi level for the upper 2DES lies in the lower spin branch of the lowest Landau level at all gate voltages used. Therefore, fractional quantum Hall features must be used as the fixed points in the density calibration. For example, in Fig. 6(a) the prom-

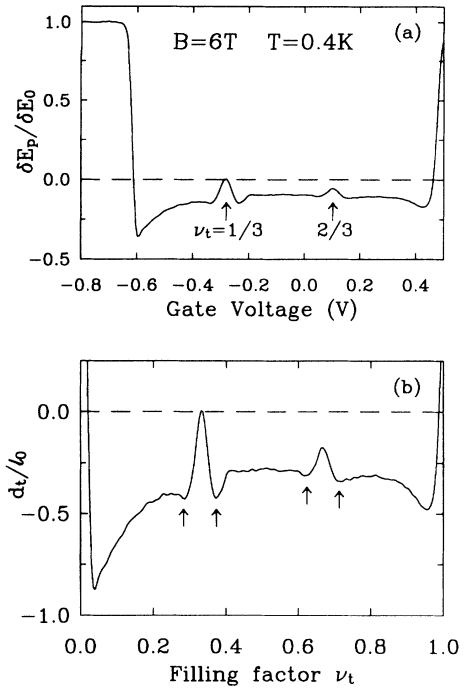

FIG. 6. (a) Differential penetration at $B=6$ T and $T=0.4$ K vs gate bias. FQHE states at $\nu_t=\frac{1}{3}$ and $\frac{2}{3}$ are highlighted. (b) Compressibility parameter d_t (divided by the magnetic length l_0) vs filling factor ν_t. The arrows denote the minima created by quasiparticle interactions. Note the truncated negative divergences as $\nu_t \rightarrow 0$ and 1.

inent local maxima in $\delta E_p/\delta E_0$ at $V_g \sim -0.28$ and 0.10 V correspond to the FQHE states at filling fractions $\nu_t=\frac{1}{3}$ and $\frac{2}{3}$, respectively, and these have been used for the density calibration for this data set. (The fitting parameters $\beta=0.923$ and $N_{\rm off}=2.0\times10^9$ cm^{-2} are virtually the same as those found at zero magnetic field and similar values were obtained at all other magnetic fields.) As at zero magnetic field, the $\delta E_p/\delta E_0$ data are converted into $d_t(\propto \partial\mu_t/\partial N_t)$ values for the equivalent narrow well structure by inverting Eq. (5). These data are displayed in Fig. 6(b) with d_t in units of the magnetic length $l_0=(\hbar/eB)^{1/2}$ (105 Å at 6 T) and the upper 2DES density N_t converted into Landau-level filling fraction $\nu_t=hN_t/eB$.

Figure 6(b) contains several qualitative features which merit discussion. Away from the peaks in $\partial\mu/\partial N$ at the $\frac{1}{3}$ and $\frac{2}{3}$ FQH states (which become positive at higher magnetic fields) the 2DES compressibility is negative throughout the extreme quantum limit $\nu_t<1$. This is not surprising since the Landau quantization quenches the kinetic energy.[35] In a noninteracting system this would leave $\partial\mu/\partial N=0$; with interactions the compressibility will be negative. (As at zero magnetic field, of course, the degree of negative compressibility will depend upon the layer thickness.) The figure also shows that the divergent trend of $\partial\mu/\partial N$ as the density goes to zero ($\nu_t \rightarrow 0$) exists at high fields just as it did at $B=0$, only it is stronger now. In this limit the total energy per electron approximates[36] that of a classical Wigner crystal for which[37] $\varepsilon_{\rm WC}=-0.7821(e^2/4\pi\varepsilon l_0)\nu^{1/2}$. This produces[16] a $\partial\mu/\partial N \propto -N^{-1/2} \propto \nu^{-1/2}$ divergence almost twice as strong as that due to simple exchange [Eq. (12)] at $B=0$. Another interesting feature here is the presence of a similar divergence as $\nu_t \rightarrow 1$. This result, which has also been seen in the Si metal-oxide semiconductor system,[17] can be understood by appealing to particle-hole symmetry. As $\nu_t \rightarrow 1$ the system may be regarded as equivalent to a dilute 2D gas of *holes* with density $1-\nu_t$. For such a system one expects $\partial\mu/\partial N \propto -(1-\nu_t)^{-1/2}$ as $\nu_t \rightarrow 1$. The observed weakness of this cutoff divergence, in comparison to the $\nu_t \rightarrow 0$ case, indicates a breaking of particle-hole symmetry. Landau-level mixing, which could be important at these low magnetic fields, is one possible source of the symmetry breaking. But even the Hartree band-bending effect, which produces a density-dependent negative contribution to $\partial\mu/\partial N$, will create an apparent particle-hole asymmetry.

The overall density dependence of $\partial\mu/\partial N$ in the extreme quantum limit reflects several factors: Hartree band bending, thickness-induced softening of the Coulomb interaction, and the many unknown features of the density-dependent total energy. In an approach designed to elucidate the gross features of the compressibility at high magnetic fields, Efros[16] has calculated $\partial\mu/\partial N$ by approximating the total energy with the interpolation formula of Fano and Ortolani.[38] This formula, appropriate to an ideally thin 2DES in the extreme quantum limit $0<\nu<1$, contains no structure due to the FQHE (i.e., no cusps) but does possess the correct limiting behavior[37] as $\nu \rightarrow 0$ and 1 and is manifestly particle-hole symmetric. The (two) fitting parameters in the formula were adjusted to closely approximate various ground-state energy estimates from exact diagonalization studies of few-electron systems. Efros[16] argues that although the formula has no first-principles validity, it represents a "backbone"[38] density dependence which should be useful when FQHE features are washed out by disorder or high temperatures. Figure 7 compares the $\partial\mu/\partial N$ calculated from the Fano-Ortolani[38] formula (dotted curve) with the experimental results at $B=11$ T. This comparison is exactly analogous to the zero-field results contained in the inset to the figure. In both cases the dotted curves represent a calculation for an ideally thin 2DES. As the figure makes plain, away from the strong FQHE structure around $\nu_t=\frac{1}{3}$ and $\frac{2}{5}$, this naive calculation agrees astonishingly well with the data. The apparent *quantitative* agreement is, however, fortuitous. It results from the approximate cancellation of the two main effects of the finite layer thickness: softened Coulomb interactions and Hartree band bending. At $B=0$ both effects were incorporated into the Hartree-Fock numerical calculations and good agreement with experiment was achieved. At high field, although lacking an analog to the finite thickness form factor of Eq. (13) which softens the electron-electron interaction, we can include the effect of the Hartree band bending. This is done (see Sec. III and the Appendix) by first solving the Schrödinger-Poisson equations to determine the quantum well energy levels ε_0 and then setting the Fermi level in

each well to $\varepsilon_F=\varepsilon_0+\frac{1}{2}\hbar\omega_c+\mu_{FO}$, where μ_{FO} is the chemical potential contribution derived from the Fano-Ortolani formula. The dashed line in Fig. 7 gives the result of these calculations. As at $B=0$, the effect of the band bending is to push the calculated $\partial\mu/\partial N$ more negative, reducing the agreement with experiment to the merely qualitative. A similar calculation for the $B=0$ case is shown in the inset; the downward shift of $\partial\mu/\partial N$ is, not surprisingly, almost quantitatively identical.[32] The softening of the Coulomb interaction will push the curves back up again; at $B=0$ this eliminates about half the band-bending effect whereas at high B, where interactions are considerably stronger, the softening apparently almost completely cancels the Hartree shift.

In this connection we note that at $\nu_t=\frac{1}{2}$ the value of $\partial\mu/\partial N$, once the Hartree shift is removed, is numerically quite small, implying the half-filled Landau level is highly compressible. For the $B=11$ and 13 T data in Figs. 7 and 8 we estimate a Hartree-corrected value of $d_t/l_0\approx-0.01$ although we stress that the systematic uncertainties in this value are considerably larger, $\sim\pm0.04$. Recent theoretical work[39] suggests that the 2DES at $\nu=\frac{1}{2}$ may be regarded as a Fermi liquid of massive composite fermions[40] in zero effective magnetic field. If disorder and interactions between the composite particles could be ignored, the compressibility would determine their mass: $\partial\mu/\partial N\propto 1/m^*$. The very small observed $\partial\mu/\partial N$ at $\nu=\frac{1}{2}$ thus points to a large mass; even with $d_t/l_0=0.04$, the estimated systematic uncertainty, the deduced mass is about 8× the bare GaAs conduction-band mass. Obviously, reduced experimental uncertainties and theoretical estimates of the effects of disorder and interactions between the composite fermions are needed in order to refine this estimate of the mass.

The most interesting qualitative features apparent in the high-field data, however, are those associated with

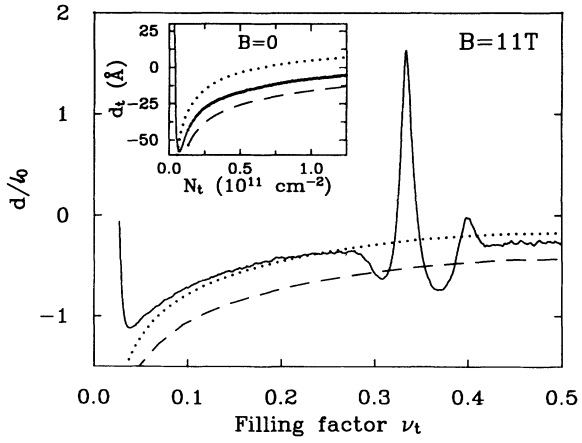

FIG. 7. Compressibility parameter d_t/l_0 vs filling factor ν_t at $B=11$ T and $T=0.4$ K. Dotted curve is the Fano-Ortolani[38] approximation employed by Efros[16] which assumes an ideally thin 2DES. Dashed curve includes the Hartree finite thickness correction but not any softening of the Coulomb interaction. Inset: Analogous comparison at $B=0$. Dotted curve represents ideally thin exchange while the dashed curve includes the Hartree correction.

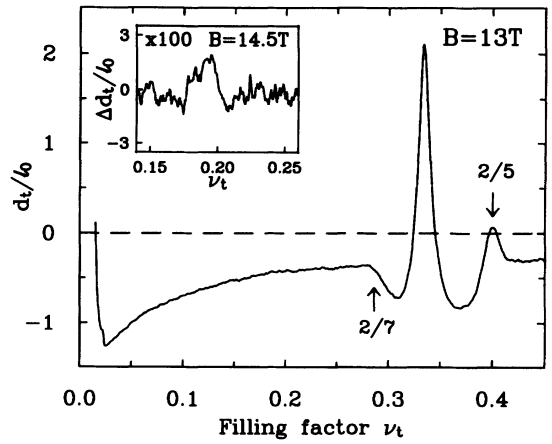

FIG. 8. Compressibility parameter d_t/l_0 vs filling factor ν_t at $B=13$ T and $T=0.4$ K. In addition to the strong $\frac{1}{3}$ state, the $\nu_t=\frac{2}{5}$ FQHE state is also easily seen. Inset: $B=14.5$ T data showing a weak feature near $\nu_t=\frac{1}{5}$. (A slowly varying background has been subtracted to obtain ths plot.)

the fractional quantum Hall effect. As Fig. 6 shows, both the $\frac{1}{3}$ and $\frac{2}{3}$ FQHE states produce local maxima in $\partial\mu/\partial N$, reflecting the "incompressibility" (i.e., the energy gap) of the liquid ground state. Although the observed strength of the FQHE peaks in $\partial\mu/\partial N$ can be enhanced significantly by increasing the magnetic field (as in Figs. 7 and 8), the maximum observed penetration we have recorded (~30% for the $\frac{1}{3}$ state at $B=13$ T) is still considerably less than unity. This is not a finite temperature effect but is instead due to the "disorder" of the 2DES. This disorder may stem from both inhomogeneous and homogeneous sources, including screened long-range density fluctuations[41] and quasiparticle lifetime broadening.[42]

Immediately adjacent to the peaks in $\partial\mu/\partial N$ at $\nu_t=\frac{1}{3}$ and $\frac{2}{3}$ are local minima, indicated by arrows in Fig. 6(b). These features are, at one level, merely indicative of downward curvature of the total energy vs density relation on each side of the upward FQHE cusp. This downward curvature has, however, a simple heuristic explanation.[12,18] Close to a precise fractional filling ν_0 (e.g., $\frac{1}{3}$) the 2DES consists of the Laughlin condensate plus a dilute gas of quasiparticles.[1] These are either quasielectrons or quasiholes, depending on whether the filling factor ν is greater or less than ν_0. In either case their density N_{qp} is proportional to $|\nu-\nu_0|$. Being charged objects the quasiparticles will interact and produce, in exact analogy to the $\nu_t\to0$ and 1 cases, new negative divergences in $\partial\mu/\partial N$, scaling as $|\nu-\nu_0|^{-1/2}$, as $\nu\to\nu_0$. Coupled with the stronger positive singularity due to the FQHE cusp itself, finite disorder will convert these quasiparticle signatures into local minima straddling a central peak. The observation of these minima represents direct thermodynamic evidence for the interacting quasiparticle excitations central to the theory of the fractional quantum Hall effect.

Increasing the magnetic field enhances the strength of the observed FQHE features in the compressibility significantly. The main panel of Fig. 8 contains $\partial\mu/\partial N$

data obtained at $B=13$ T, while the inset shows a restricted set of 14.5-T results (from which a smooth background has been subtracted). Both data sets were taken at $T=0.4$ K. At these fields the main $\nu_t=\frac{1}{3}$ peak is strongly positive, the differential penetration reaching $+30\%$ at $B=13$ T. A strong peak is also observed for the $\nu_t=\frac{2}{5}$ state (at lower magnetic field the $\frac{3}{5}$ state is seen as well). Less obvious at 13 T is the $\frac{2}{7}$ state, although a weak maximum has been detected there at $B=14.5$ T (not shown in the inset). The $B=14.5$ T data were obtained at the increased measurement frequency of 23 Hz. This was done to reduce the preamplifier noise and hopefully detect a compressibility signature for the $\nu_t=\frac{1}{5}$ state. At this high frequency the data very near $\frac{1}{3}$ filling were polluted by finite conductivity effects but over the range $0.32>\nu_t>0.03$, including the $\frac{2}{7}$ and $\frac{1}{5}$ states, they were not. As the inset shows, a clearly defined maximum is found close to $\nu_t=\frac{1}{5}$. While this is almost certainly the FQHE $\frac{1}{5}$ state, it is slightly displaced in density ($\delta\nu_t\sim0.01$). The reason for this is unknown but it is most probably due to uncertainties in the gate voltage-to-density calibration. (At these high fields the $\frac{1}{3}$ and $\frac{2}{5}$ states are used as fixed points and they are unfortunately rather close together.) In any case, the peak near $\frac{1}{5}$ filling is fully 100 times smaller than the corresponding one at $\nu_t=\frac{1}{3}$.

Intriguingly, the observed $\partial\mu/\partial N$ shows the characteristic signature of strong electron-electron interactions, i.e., a tendency toward divergence at low density, down to a filling factor of about $\nu_t^{\min}\approx0.025$ while, at the same time, exhibiting no significant FQHE features for $\nu_t<2/7$. This suggests that the FQHE, while dominating the electrical transport parameters, really represents rather weak additional correlations in an already strongly interacting system. This view is consistent with the recent observation[43] of a deep gap in the tunneling density of states of the 2DES that exists over wide ranges of filling factor. This gap is a purely collective effect and yet it is only weakly affected by the FQHE.

B. Chemical potential jump at $\nu=\frac{1}{3}$

A discontinuity $\Delta\mu$ in the chemical potential at certain magic densities is perhaps the single most important prediction of the theory of the FQHE. Heretofore $\Delta\mu$ has only been inferred, almost exclusively[44] through its theoretical connection to the measured excitation gap E_g extracted from the thermally activated transport coefficient ρ_{xx}. For the $\nu=p/q$ FQH states the predicted ratio $\Delta\mu/E_g$ is just q, the inverse of the quasiparticle charge.[1] As mentioned in the Introduction, transport determinations of E_g are insensitive to localized states in the gap, measuring instead of mobility gap between extended quasiparticle states. In contrast, by simply integrating the observed compressibility $\partial\mu/\partial N$ we can extract the first thermodynamic determinations of $\Delta\mu$. These results reflect all electronic states, both extended and localized.

Figure 9(a) illustrates the temperature dependence of the compressibility around the $\nu_t=\frac{1}{3}$ and $\frac{2}{5}$ FQHE states

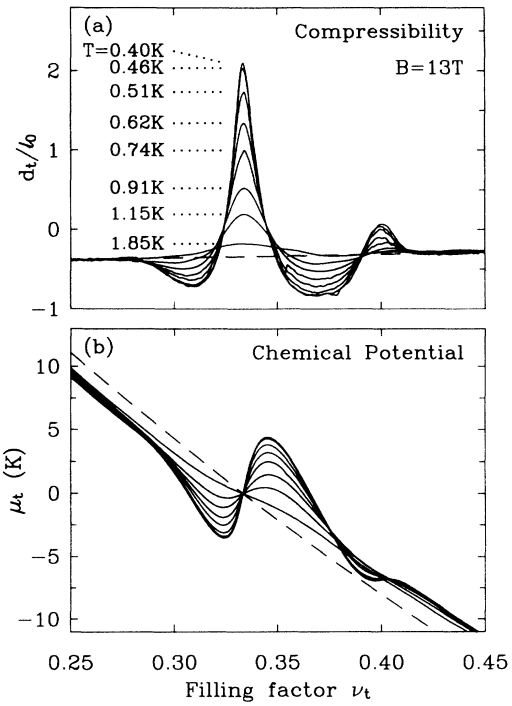

FIG. 9. (a) Temperature dependence of $\nu_t=\frac{1}{3}$ FQHE compressibility signature at $B=13$ T. The nearly horizontal dashed line is a fit to the high-temperature background compressibility. (b) Chemical potential around the $\nu_t=\frac{1}{3}$ FQHE obtained by integrating the compressibility data in (a). Dashed line is the integral of the background compressibility.

at $B=13$ T. Significant temperature dependence persists to below 0.5 K, although the data suggest a leveling off below 0.4 K. It was very difficult to obtain reliable thermodynamic data (for the $\nu_t=\frac{1}{3}$ peak) below 0.36 K at this magnetic field owing to the rapidly falling sheet conductivity. At temperatures above about 2 K the peak at $\nu_t=\frac{1}{3}$ disappears leaving only a smooth negative background compressibility. The dashed line is an estimate of that background obtained by a linear fit to the $T=1.85$ K data in the windows $0.25<\nu_t<0.27$ and $0.43<\nu_t<0.45$. The chemical potential, shown in Fig. 9(b), is obtained by integration:

$$\mu_t=\int\frac{\partial\mu_t}{\partial N_t}dN_t=\frac{e^2}{2\pi\varepsilon l_0}\int\frac{d_t}{l_0}d\nu_t\ . \tag{14}$$

The constant of integration is chosen so that $\mu_t=0$ at $\nu_t=\frac{1}{3}$. The dashed line in Fig. 9(b) is the integral of the linear fit to the high-temperature background compressibility. From the data in Fig. 9(b) we can extract $\Delta\mu_t$, the jump in the chemical potential for the $\frac{1}{3}$ FQHE state at $B=13$ T. These results are denoted by the solid dots in Fig. 10. The open circles in the figure show the magnetic-field dependence of $\Delta\mu_t$ at the fixed low temperature of $T=0.41$ K. [For both data sets, the $\Delta\mu_t$ values are normalized by the typical Coulomb energy $e^2/4\pi\varepsilon l_0\approx51K\sqrt{B(\text{tesla})}$.] To assign numerical values to $\Delta\mu_t$, a smooth density-dependent background was first

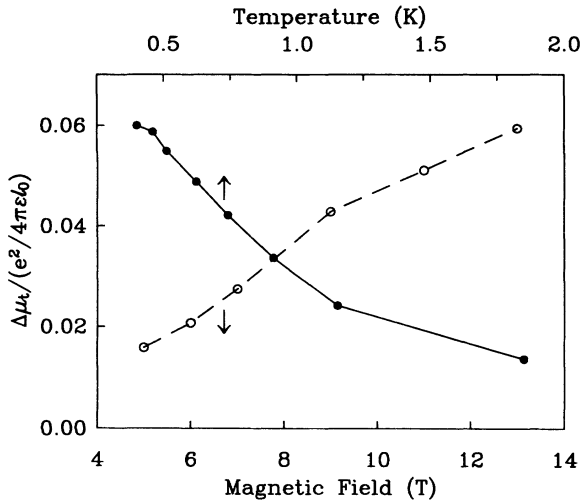

FIG. 10. Chemical potential jump at $\nu_t=\frac{1}{3}$ vs temperature at $B=13$ T and vs magnetic field at $T=0.4$ K. These jumps, displayed in units of $e^2/4\pi\varepsilon l_0$, include the background subtraction described in the text.

subtracted from the integrated $\partial\mu/\partial N$. For the data in Fig. 9(b) this background is just the dashed line, the integral of the linear fit to the high-temperature compressibility just described. (A similar background subtraction is performed for the $T=0.41$ K magnetic-field-dependent $\Delta\mu_t$ values.) The jump $\Delta\mu_t$ is then set to the difference between the local maximum and minimum in this background-subtracted chemical potential immediately adjacent to $\nu_t=\frac{1}{3}$. The efficacy of this background subtraction scheme is aided by the relative sharpness of the observed FQHE features. As outlined in the Appendix this analysis has been validated by applying it to numerically simulated $\delta E_p/\delta E_0$ data in which a known chemical potential jump has been imposed.

C. Analysis and discussion

The predicted[1] chemical potential discontinuity for the $\nu=\frac{1}{3}$ FQHE state in an ideal 2DES, in the limit of very high magnetic field, is approximately $\Delta\mu=0.3e^2/4\pi\varepsilon l_0$. As the data in Fig. 10 make clear, the observed chemical potential jump never exceeds 20% of this ideal value. Similarly, the maximum value of d_t/l_0 observed at $\nu_t=\frac{1}{3}$ is only ≈ 2.4 (at $T=0.4$ K and $B=13$ T and with the Hartree contribution[32] removed). This value implies that the effective density of states $\partial N/\partial\mu$ in the center of the FQHE gap is still 15% of that in an ideal noninteracting 2DES at $B=0$. These results, coupled with the obvious smearing of the "discontinuity" in chemical potential and the clear indication (from Fig. 10) that higher magnetic fields would produce larger values of $\Delta\mu_t/(e^2/4\pi\varepsilon l_0)$, suggest a substantial role for disorder.

The present compressibility measurements average over the entire sample area (210×210 μm) and are therefore quite sensitive to long-range fluctuations in the 2DES density. Such density variations can arise both from statistical fluctuations in the ionized donor distribution[41] but also from nonuniformities in the MBE growth of the sample. In order to investigate the effect of this inhomogeneous broadening on the observed $\partial\mu/\partial N$ we have to assume a distribution function and adopt a specific model for the density dependence of the total energy $E_{\rm tot}(N)$ near the FQHE singularity. For simplicity we will take the density distribution to be a simple Gaussian[18] about the average density N_0

$$P(N)=(2\pi\sigma_N^2)^{-1/2}\exp[-(N-N_0)^2/2\sigma_N^2]\ . \qquad (15)$$

This assumption for $P(N)$ ignores the effects of screening in the FQHE regime. Pikus and Efros[41] have shown that the Gaussian assumption is only good if the FQHE gap is small in comparison to the mean fluctuations of the ionized donor potential and that this probably is not the case in our samples. In their model the density distribution exhibits a percolating network of strips of finite width in which the density is pinned to magic FQHE values. For the Gaussian, of course, these strips are just contour lines with zero width. We employ the Gaussian for simplicity and refer the reader to Pikus and Efros's paper[41] for the more sophisticated model.

The total energy in the proximity of an FQHE state at $\nu_0=1/m$ is modeled[45] as a cusp plus a term to account for quasiparticle interactions. With energy in units of $e^2/4\pi\varepsilon l_0$ the total energy (per unit area) is

$$E_{\rm tot}(\nu)=E_{\rm tot}(\nu_0)+\varepsilon^{\pm}N_{\rm qp} -0.7821m^{-2}(2\pi l_0^2)^{1/2}N_{\rm qp}^{3/2}\ , \qquad (16)$$

where $N_{\rm qp}=m|\nu-\nu_0|/(2\pi l_0^2)$ is the number of quasiparticles of charge $e^*/e=1/m$ per unit area and ε^+ (ε^-) is the so-called "gross" quasielectron (quasihole) energy.[46] The term linear in $N_{\rm qp}$ gives the cusp in $E_{\rm tot}$ and a chemical potential ($\mu=\partial E_{\rm tot}/\partial N=2\pi l_0^2\partial E_{\rm tot}/\partial\nu$) discontinuity $\Delta\mu=m(\varepsilon^++\varepsilon^-)$ at $\nu=\nu_0$. The last term in Eq. (16) approximates the quasiparticle interactions with the same Wigner crystal estimate[37] used for the electrons in the $\nu_t\to 0$ limit only modified appropriately for the quasiparticle charge and density. A similar formula was employed by Pikus and Efros[41] only their interaction term differs from ours by a factor of $m^{3/2}$.

Figure 11 contains examples of the calculated $d/l_0\propto\partial\mu/\partial N$ and chemical potential μ for the $\nu_0=\frac{1}{3}$ FQHE state. Both the solid and dotted lines result from convolving the total energy in Eq. (16) with a Gaussian density distribution $P(N)$ of width $\sigma_N/N_0=0.03$ and then taking the appropriate density derivatives to determine d/l_0 and μ. The only difference between the two curves is that the quasiparticle interaction term was omitted in the dotted line case. It is obvious from the figure that these interactions have a major impact on the results. As expected they produce satellite minima adjacent to the main $\partial\mu/\partial N$ peak but they also have a significant effect on the peak height and the magnitude of the smoothed jump in the chemical potential. The reason for this is apparent from the dashed curve in Fig. 11(b) which shows the chemical potential in the absence of smoothing. The quasiparticle interactions create sharp

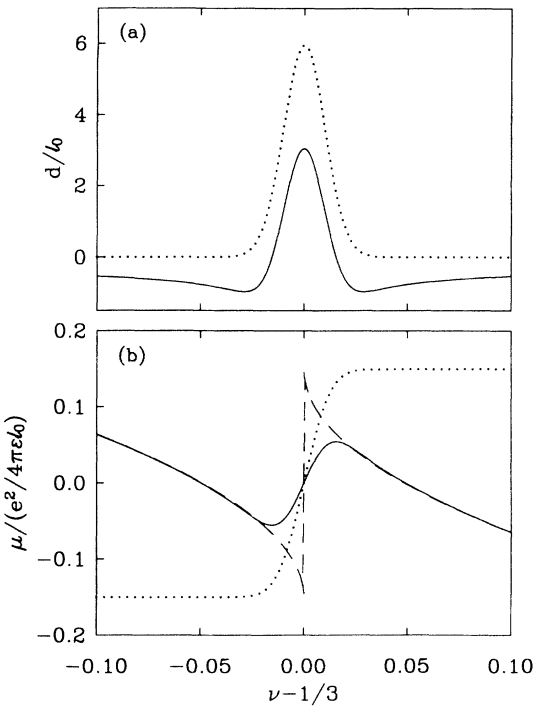

FIG. 11. (a) FQHE compressibility parameter d/l_0 vs $\nu-\frac{1}{3}$ calculated using the model described in the text including convolution with a Gaussian density distribution of width $\sigma_N/N=0.03$. Solid curve includes quasiparticle interactions, dotted curve omits them. (b) Calculated FQHE chemical potential signature. The dashed curve omits the density averaging.

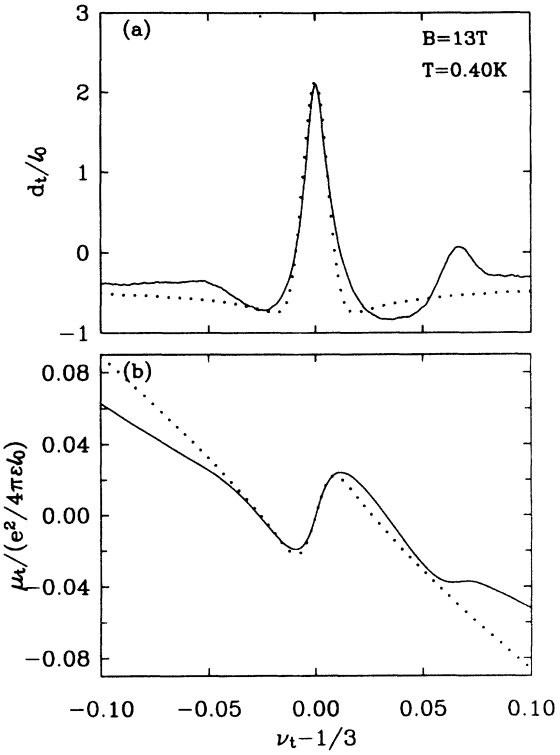

FIG. 12. Comparison of observed compressibility and chemical potential data (solid curves) around the $\nu_t=\frac{1}{3}$ FQHE state with the theoretical model including a Gaussian density distribution of width $\sigma_N=1.8\times10^9$ cm^{-2} and a phenomenological suppression parameter $F=0.394$. The theory curves include the estimated (Ref. 32) Hartree shift.

peaks in μ at the discontinuity and these will be easily wiped out by density fluctuations, finite temperature, or any other source of disorder.

We have not found it possible to simultaneously fit the width and amplitude of the observed compressibility peak with the single parameter σ_N. Reasonable fits can be obtained, however, after simply multiplying the total energy in Eq. (16) by an *ad hoc* suppression parameter F. Figure 12 compares the $B=13$ T, $T=0.4$ K data with this generalized model. The calculated $\partial\mu/\partial N$ and chemical potential are shown as dotted lines. To arrive at these curves we have simply adjusted σ_N to give the correct width for the peak and then chosen F to fit the amplitude. (The theory curve also incorporates our best estimate[32] of the Hartree band bending contribution the compressibility but this has no impact on the fitted width and amplitude of the peak.) For the data in Fig. 12 we found $\sigma_N=1.8\times10^9$ cm^{-2} and $F=0.39$. This value for σ_N is reasonable, being about half that expected[41] from statistical fluctuations in a random donor distribution (set back 1400 Å from the 2DES) with concentration equal to that of the ungated 2DES. In spite of the many approximations within the theoretical model (neglect of higher-order fractions, an oversimplified quasiparticle interaction term, etc.) the "fit" shown in Fig. 12 seems reasonable. The model is employed merely for the extraction of two simple but important numbers from the data: the amplitude ($\propto F$) and the width (σ_N) of the FQHE compressibility signature.

Both the finite thickness of the 2DES and the mixing in of higher Landau levels contribute slightly to the suppression parameter F. There have been numerous theoretical estimates of the thickness-induced FQHE gap suppression, mostly for the so-called Fang-Howard wave function.[1] In quantum wells, however, the subband wave function does not possess the long tail characteristic of heterojunctions and consequently the thickness effects are reduced. We have estimated the effect in quantum wells by calculating the Coulomb pseudopotentials V_m (in the lowest Landau level) for an ideal infinite square well, using the result of Price.[29] The V_m represent the Coulomb repulsion between a pair of electrons with orbital angular momentum m. Following a suggestion of MacDonald[47] we assume the quasiparticle gap for the $\nu=\frac{1}{3}$ state is proportional to the difference $V_{1,3}\equiv V_1-V_3$. (In the Fang-Howard case this assumption agrees well with the existing literature.[1]) We find that the ratio γ of $V_{1,3}$ for our 200-Å-wide quantum wells to the ideally thin value ranges from a minimum of $\gamma=0.865$ at $B=13$ T up to 0.932 at $B=5$ T. The effect of Landau-level mixing on the gap has been estimated by Yoshioka.[48] This effect, which depends upon the ratio $(e^2/4\pi\varepsilon l_0)/\hbar\omega_c$ suppresses the gap by typically 10–20 % in our case. As the mixing becomes less important at high fields where the finite

thickness suppression is greatest, the combined effect is roughly independent of field. Redefining the parameter γ to include both effects, we find $\gamma \approx 0.78$ for $5 < B < 13$ T. The small values of F (<0.4) required for fitting the compressibility data therefore suggest an additional source of disorder beyond simple inhomogeneous broadening.

Figure 13 summarizes the results of the fits of the theoretical model to the $T=0.4$ K data, assuming the ideal quasiparticle gap at $\nu=\frac{1}{3}$ is $0.10e^2/4\pi\varepsilon l_0$. These "fits" are not least-squares in any sense, we have merely adjusted σ_N and F till the model matches the amplitude and full width at half maximum found in the data. [A smooth background is first subtracted from the data; see the discussion of Figs. 9 and 10. There generally remains a small ($\Delta d_t/l_0 \sim 0.05$) vertical offset between the fit and the background-subtracted data, which we ignore.] The quality of the fits is comparable to that shown in Fig. 12. From 13(a) we conclude that the inhomogeneous broadening parameter σ_N remains near 2×10^9 cm^{-2} independent of magnetic field. This independence is expected since the density fluctuations are set by the donor distribution and this not altered when the gate is used to change the 2DES density. In Fig. 13(b) the solid dots show that the suppression parameter F^* is strongly field dependent. ($F^* \equiv F/\gamma$, so the figure represents the suppression after removing the finite thickness and Landau-level mixing effects.) Not surprisingly, the field dependence of F^* is roughly the same as that of the normalized chemical potential jump shown in Fig. 10.

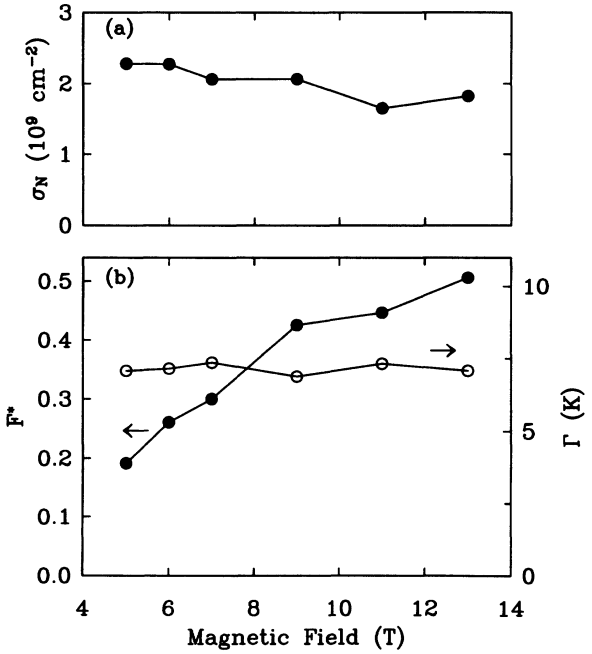

FIG. 13. Results of the fits of the $\frac{1}{3}$-state compressibility peak at $T=0.4$ K to the theoretical model vs magnetic field. (a) Width of Gaussian density distribution. (b) Solid dots: Phenomenological suppression parameter F^*. ($F^*=F/\gamma$, with $\gamma \approx 0.78$ is the combined finite thickness/Landau-level mixing gap suppression.) Open dots: Homogeneous broadening parameter Γ determined from F^* via Eq. (17).

The physical origin of the suppression of the FQHE compressibility signatures beyond simple inhomogeneous broadening is not well understood. Conceivably the assumption of a Gaussian density distribution obscures the more subtle aspects of the inhomogeneity and, were these accounted for, agreement with theory could be obtained without resorting to a phenomenological suppression parameter. Pikus and Efros[41] have examined this issue carefully and have shown that the Gaussian model is indeed oversimplified. Their calculations show that the deviations from the Gaussian actually *enhance* the compressibility peak, at least for a given random donor distribution. No doubt by adjusting the donor fluctuations their model would yield better agreement with experiment than the simple Gaussian approach. This might be justified since the fitted σ_N values are smaller than the estimate[41] based on a random donor distribution.

Another possibility is that the suppression parameter F^* reflects some kind of scattering induced lifetime broadening of the quasiparticle states. For example, MacDonald, *et al.*[42] considered the disorder broadening of the magnetoroton excitations. Over the years this idea has been applied to the analysis of the quasiparticle gap determined from the activated temperature dependence of the diagonal resistivity.[49] In this phenomenological approach the observed energy gap $\Delta_{\rm exp}(B)$ is assumed to be smaller than the disorder-free gap $\Delta(B)$ by some constant amount: $\Delta_{\rm exp}(B)=\Delta(B)-\Gamma$. The parameter Γ represents the width of the broadened quasiparticle states. Adapting this to the present context we write

$$\Delta_{\rm exp}(B)=F^*\gamma\Delta_0(B)=\gamma\Delta_0(B)-\Gamma\ , \tag{17}$$

where γ is the combined finite thickness and Landau-level mixing gap suppression and $\Delta_0(B)\approx 0.10e^2/4\pi\varepsilon l_0 \propto \sqrt{B}$ is the predicted energy gap for the $\nu=\frac{1}{3}$ FQHE state in a clean and ideally thin 2DES. The open circles in Fig. 13(b) represent the values of Γ determined by applying Eq. (17) to the fitted F^* and calculated γ values. In spite of the strong field dependence of F^*, the broadening parameter is roughly independent of magnetic field, $\Gamma \approx 7.4$ K $=0.64$ meV, suggesting that the simple homogeneous broadening model expressed by Eq. (17) is at least plausible. The magnitude of Γ is about $4\times$ larger than the zero-field lifetime broadening determined in interlayer tunneling studies on similar samples.[50] Little is known about the physics of quasiparticle scattering and thus the magnitude of Γ is not readily interpreted. Nevertheless, since the observed compressibility at $\nu=\frac{1}{3}$, while nonzero, is considerably smaller than at zero magnetic field, the donor impurity potential is less well screened. One might thus expect relatively strong quasiparticle scattering.

We also note that the tiny magnitude of the compressibility signature at $\nu=\frac{1}{5}$ argues against models including only inhomogeneous broadening. The estimated[1] quasiparticle gap for the $\frac{1}{5}$ state is about one-fourth of the $\frac{1}{3}$-state gap, making the chemical potential jump 40% as large as for $\nu=\frac{1}{3}$. If this is the case, and knowing that σ_N is essentially independent of density, a strong compressibility feature should be seen at $\frac{1}{5}$. On the other

hand, at 14.5 T (appropriate to the inset to Fig. 8) the predicted $\nu=\frac{1}{5}$ excitation gap is roughly 5 K, close to the broadening parameter $\Gamma\sim 7$ K extracted from the $\frac{1}{3}$-state analysis. The crude equality of these numbers plausibly explains the near absence of the $\nu=\frac{1}{5}$ state and supports the view that simple inhomogeneous broadening does not fully represent the disorder in the sample.

Conceivably, the observed gap suppression might not be due to disorder at all, resulting instead from some unappreciated new physics. One interesting speculative possibility is that the second 2DES layer is somehow involved. A simple way in which this might occur would be in the second layer's screening of the electron-electron interaction in the FQHE layer. If the second layer acts as a perfect metal then the positive image charges for each electron in the FQHE layer soften the long-distance Coulomb repulsion and this should reduce the gap.[51,52] Since the Laughlin $\frac{1}{3}$ state depends mostly on the short-range part of the interaction the image plane has to be nearby for there to be much effect. We have estimated this by again calculating the V_1-V_3 pseudopotential difference for such a screened interaction. Taking the distance to the image plane to be 375 Å, the quantum well center-to-center spacing, the calculated gap suppression is only 2% at $B=13$ T rising to 6% at 5 T. (These results are in good agreement with those of Sivan.[51]) If one assumes that the relevant spacing is just the barrier width, 175 Å, suppressions of 11 and 26 % are obtained at these magnetic fields. Thus, while probably not strong enough to explain the present data, it would be very interesting to search for this effect in samples with more closely spaced layers.

V. CONCLUSION

This paper has been devoted to the extraction of quantitative information about electron-electron interactions in 2D systems using a thermodynamic probe, the compressibility. We have shown that it is possible to attain quantitative agreement between theory and experiment at zero magnetic field by taking account of the 2D exchange energy and the smaller, yet important, effects of the finite thickness of the 2D sheets. At high magnetic field, in the fractional quantum Hall regime, we have used the strong compressibility signatures observed at the $\nu=\frac{1}{3}$ state to learn several things about this novel quantum fluid. First, we have demonstrated the importance of quasiparticle interactions. At the qualitative level these interactions produce the satellite minima adjacent to the FQHE compressibility peak while on the quantitative side they have a significant impact on the shape and magnitude of the observed chemical potential jump in real samples where inhomogeneous broadening is important. By fitting our data to a simple model of the FQHE total energy we have extracted both a measure of the inhomogeneous density distribution in our sample and the magnitude of an apparently distinct suppression mechanism. While this latter effect may be interpreted in terms of a homogeneous quasiparticle lifetime broadening, its precise origin remains puzzling.

There are numerous avenues for future work in this area. One possibility would be to try to determine the quasiparticle charge from the ratio of the chemical potential jump to the quasiparticle excitation gap. While the latter is usually determined from transport measurements, the temperature dependence of the peak compressibility in an FQHE state should also reflect this gap. An advantage of this approach would be its *in situ* nature. When better samples become available the weaker FQHE states could also be studied, perhaps allowing a test of the recent suggestions[53] that the states in the sequence $\frac{1}{3}$, $\frac{2}{5}$, $\frac{3}{7}$, . . . share the same chemical potential jump. Another possibility would be to investigate the compressibility near the Wigner crystal transition. Finally, double layer systems with thinner barriers offer interesting possibilities as well. In addition to possible instabilities at very low density[26] there is the general issue of how interlayer correlations might be studied via compressibility.

ACKNOWLEDGMENTS

It is a pleasure to thank S. Das Sarma, B. I. Halperin, Song He, R. L. Willett, X. Zhu, and especially M. S. Hybertsen, for numerous very useful discussions. We also thank A. L. Efros and F. G. Pikus for their interest in these experiments and for sharing with us the results of their calculations prior to publication. Thanks also to Jun Hu for providing us with initial self-consistent LDA subband calculations; these were very helpful in setting up our own numerical procedures. Finally, we wish to thank A. H. MacDonald for his extensive theoretical help and general interest in this work.

APPENDIX: NUMERICAL PROCEDURES

Self-consistent DQW solver

In order to predict the differential penetration $\delta E_p/\delta E_0$ in a given circumstance we solve for the equilibrium charge density in each quantum well in a double layer structure for a given distribution of neutralizing background charge. This background charge is considered to be localized in two planes, one above the DQW and one below it, mimicking the actual doping of the sample. The gate, which is deposited on the sample top surface, contributes additional background charge but this can, without loss of generality, simply be included as part of the upper donor concentration. We assume that the individual quantum wells are sufficiently separated that they may be regarded as quantum mechanically independent and that no charges other than those in the donor sheets (and gate) and in the quantum wells (the 2DES's) need be considered. Let D_t and D_b be the areal concentrations of the top and bottom donor sheets and N_t and N_b the 2DES concentrations in the two quantum wells.

Ignoring, for the moment, electron-electron interactions beyond the Hartree approximation, for a given D_t and D_b the Schrödinger and Poisson equations are first solved self-consistently for each quantum well separately, assuming some definite partitioning of the total 2DES charge available (D_t+D_b) between the two wells. For

each well the net confining potential is of the form

$$V(z)=V_{QW}(z)+V_B(z)+V_H(z,\phi(z)) , \quad \text{(A1)}$$

where V_{QW} is the quantum well defined by the conduction-band offset of GaAs and $Al_{0.3}Ga_{0.7}As$, here assumed to be 250 meV, V_B is the net (linear) potential due to the background charge, which includes both positive donor sheets *and the 2DES in the other quantum well.* The last term, V_H is the space charge, or Hartree, potential which depends upon the subband wave function $\phi(z)$. This last term is calculated from integrating the Poisson equation.[33] We assume simple parabolic bands with effective mass $m^*/m_0=0.067$ and take the dielectric constant to be $\varepsilon=12.6\varepsilon_0$; any discontinuities in these parameters at the quantum well interfaces are ignored. Starting by assuming the 2DES charge is spread uniformly across the quantum well, the Schrödinger equation is solved to obtain the ground subband wave function $\phi(z)$ and energy ε_0 (no higher levels are ever populated). The Hartree potential is then recomputed and the process repeated until convergence has been achieved. Knowing the ground subband energy in each quantum well, the chemical potentials are then calculated, in the Hartree approximation and at zero magnetic field, by adding on the Fermi energies $\pi\hbar^2N_{t,b}/m^*$. Taking proper account of the electric field within the barrier layer, these two chemical potentials are then compared. If they do not match charge is transferred from one well to the other and the whole process repeated. This interwell self-consistency loop proceeds until final convergence is achieved.

Many-body effects have been incorporated into this procedure in two different ways, the local-density approximation (LDA) and a "thickened" 2D Hartree-Fock approximation. In the LDA an additional term $V_{xc}(z)$ is added to the potential in Eq. (A1). We have employed the Hedin-Lundqvist[34] LDA exchange-correlation functional in our calculations. With this term included the calculated subband energy ε_0 contains the many-body effects, and the chemical potential is found by simply adding on the Fermi energy $\pi\hbar^2N_{t,b}/m^*$. In the thickened 2D Hartree-Fock approximation we calculate the 2D exchange contribution to the chemical potential taking into account the thickness of the 2DES with a density-dependent form factor.[28] (This form factor is discussed in detail at the end of this appendix.) At each step in the interwell charge-transfer loop these exchange contributions are added to the noninteracting chemical potential.

Calculation of differential penetration

Once the densities $N_{t,b}$ are determined for a wide range of top donor concentrations D_t (the bottom donor density D_b is kept fixed throughout) the differential penetration is evaluated as follows. A small variation δD_t (due to a small change in gate voltage) produces a small change $\delta E_0=(e/\varepsilon)\delta D_t$ in the electric field between the upper donor sheet and upper quantum well. Some of this electric field penetrates the upper well and impinges upon the lower. The variation in the penetrating field δE_p is proportional to the change in the bottom 2DES density: $\delta E_p=(e/\varepsilon)\delta N_b$. From charge neutrality ($D_t+D_b=N_t+N_b$) we have

$$\delta E_p/\delta E_0=G/(1+G);\quad G=\delta N_b/\delta N_t . \quad \text{(A2)}$$

The derivative G is evaluated either as a finite difference or computed analytically after first fitting the paired N_b and N_t values to a sensible function $N_b=H(N_t)$.

Figure 14 presents typical results from the LDA. In Fig. 14(a) the calculated 2DES densities are plotted vs the top donor layer density D_t which acts as the "gate." (For these data the bottom donor density was set to $D_b=0.8\times10^{11}$ cm^{-2}, but the final $\delta E_p/\delta E_0$ results hardly depend on this value.) As the figure shows, the upper 2DES density is roughly linear in D_t. By contrast the bottom layer density, while changing little in magnitude, *increases* as the top layer is being depleted of carriers. This overscreening reflects the negative compressibility of the top 2DES. In Fig. 14(b) the same data are replotted as N_b vs N_t. This is appropriate since the penetration effect is governed by the upper 2DES density, not the donor concentration. The solid line in Fig. 14(b) is a least-squares fit of the function

$$H(N_t)=a_1N_t^{1/2}+a_2+a_3N_t+a_4N_t^2+a_5N_t^3 \quad \text{(A3)}$$

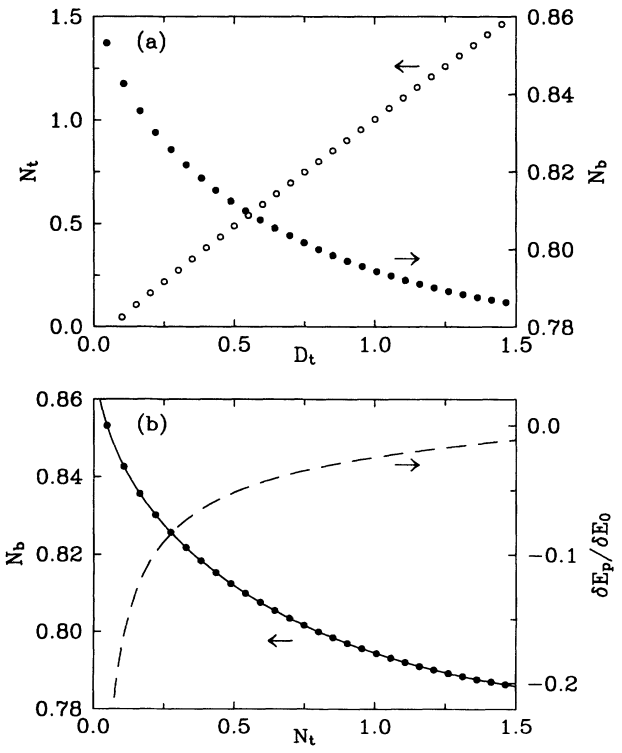

FIG. 14. Results of LDA calculations. (a) 2DES densities in the top (N_t, open dots) and bottom (N_b, solid dots) quantum wells vs the top donor layer density D_t, all in units of 10^{11} cm^{-2}. (b) Solid dots: Calculated bottom 2DES density N_b vs top 2DES density N_t. Solid line through points is a least-squares fit of the function $H(N_t)$. Dashed line is the computed differential penetration $\delta E_p/\delta E_0$.

to the computed N_b values. Differentiating to obtain $G(N_t)=H'(N_t)$ produces, via Eq. (A2), the calculated differential penetration $\delta E_p/\delta E_0$ shown as a dashed line in Fig. 14(b). Exactly as with experimental data these $\delta E_p/\delta E_0$ values can be converted into the compressibility parameter d_t for the equivalent narrow well model by inverting Eq. (5). The d_t values for this example are represented by the dashed line in Fig. 5. [As described in the text, the value of d_b is replaced by the constant evaluated using Eq. (5) at balance where $N_t=N_b$ and thus $d_b=d_t$.]

Determination of chemical potential jumps

The chemical potential jumps for the $\nu=\frac{1}{3}$ FQHE were evaluated by integrating the "equivalent" narrow well compressibility parameter d_t found by inverting Eq. (5). We here validate this analysis by applying it to artificial data constructed using the numerical procedures outlined above. Specifically, we simulate the jump of the Fermi level between the two lowest Landau levels at filling factor $\nu=2$ and calculate the resulting $\delta E_p/\delta E_0$. These "data" are then analyzed just as the experimental data. We assume that in a perpendicular magnetic field the in-plane and z motion remain decoupled. Electron-electron interactions are ignored except for the Hartree self-consistent potential. The Fermi level is assumed to remain fixed at $\frac{1}{2}\hbar\omega_c$ above the ground subband energy ε_0 until the 2DES density N_t exceeds $N^*=1.0\times10^{11}$ cm^{-2} where it jumps to $3/2\hbar\omega_c$. For GaAs this corresponds to a magnetic field of $B=2.07$ T where $\hbar\omega_c=3.60$ meV. The Landau-level contribution to the chemical potential is taken to be

$$\mu_{\rm LL}=\tfrac{1}{2}\hbar\omega_c(2+\tanh[(N_{t,b}-N^*)/\sigma_0]) . \quad \text{(A4)}$$

The jump has been smoothed out for convenience, taking $\sigma_0=N^*/40$. The bottom donor density is set again to 0.8×10^{11} cm^{-2} and, as a consequence, the lower 2DES remains in the lowest Landau level throughout. Figure 15(a) shows both the calculated lower 2DES density and differential penetration $\delta E_p/\delta E_0$ vs top 2DES density N_t. The latter was computed via Eq. (A2) after fitting the $N_b(N_t)$ data to the form

$$H(N_t)=a_1+a_2(N_t-N^*)+a_3(N_t-N^*)^2 +a_4\tanh[(N_t-N^*)/\sigma] . \quad \text{(A5)}$$

The line running through the solid dots in Fig. 15(a) is the fitted $H(N_t)$ function. Figure 15(b) shows the "equivalent narrow well" compressibility parameter d_t determined by inverting Eq. (5) and the deduced chemical potential obtained by integration as in Eq. (14). Note that away from the peak in d_t the compressibility is slightly negative. This is just the Hartree band-bending effect described in the text. The dashed line is a linear fit to this background compressibility away from the peak. To obtain the chemical potential μ_t^* shown, this background is subtracted from d_t prior to the integration. This is exactly the same procedure applied to the actual experimental data around the $\nu=\frac{1}{3}$ FQHE. After this subtraction the deduced chemical potential jump is 3.60 meV in exact agreement with $\hbar\omega_c$.

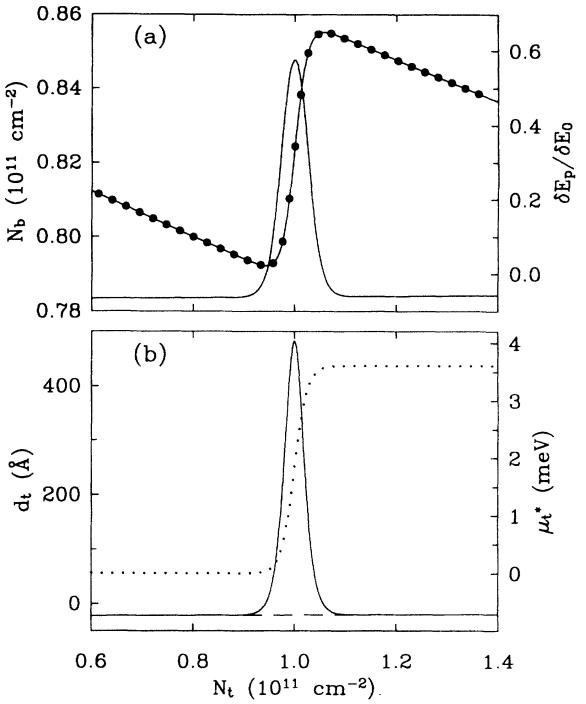

FIG. 15. Simulation of Fermi-level jump between two Landau levels. (a) Solid dots: Calculated lower 2DES density N_b vs upper 2DES density N_t. Line through points is the least-squares fit to the function $H(N_t)$. The broadened peak is the calculated differential penetration $\delta E_p/\delta E_0$. (b) Solid curve: Compressibility parameter d_t from equivalent narrow well analysis. Dotted curve: Background subtracted chemical potential. The measured jump is 3.60 meV, in exact agreement with $\hbar\omega_c$.

Exchange energy form factor

The exchange energy at zero magnetic field for electrons in the ground subband of a quantum well of width w is numerically smaller than for the ideally thin case. Defining the form factor $F(r_s,\phi(z))$ as the ratio of the thickened to the ideal 2D exchange energy per electron we have, following Stern,[28]

$$F(r_s,\phi(z))\equiv\frac{\varepsilon_{\rm ex}(w)}{\varepsilon_{\rm ex}(0)} =\tfrac{3}{2}\int_0^1 f(2k_Fx)[\cos^{-1}(x)-x\sqrt{1-x^2}]dx , \quad \text{(A6)}$$

where the Fermi wave vector $k_F=(2\pi N)^{1/2}=\sqrt{2}/a_0r_s$ and the function $f(2k_Fx)$ depends upon the subband wave function $\phi(z)$:

$$f(q)=\int\int|\phi(z)|^2|\phi(z')|^2\exp(-q|z-z'|)dz\,dz' . \quad \text{(A7)}$$

Price[29] has evaluated Eq. (A7) for the case of an infinite square well where $\phi(z)=(2/w)^{1/2}\sin(\pi z/w)$ obtaining

$$f_{\mathrm{SQW}}(q)=\frac{y+3g(y)}{y^2+4\pi^2}-\frac{(y^2-4\pi^2)g(y)}{(y^2+4\pi^2)^2}+\frac{2}{y}\left[1-\frac{g(y)}{y}\right], \tag{A8}$$

where $g(y)=(1-e^{-y})$ and $y=qw$. With this result we have numerically integrated Eq. (A6) and fitted the results, which depend only on the single variable $\zeta=w/a_0r_s$, to a third-order polynomial valid over the range $(0<x<3.5)$:

$$F_{\mathrm{SQW}}(\zeta)=1-0.16851\zeta+0.027669\zeta^2-0.0024392\zeta^3\ . \tag{A9}$$

With this result we can evaluate the exchange contribution to the chemical potential via $\mu_{\mathrm{ex}}=\partial(N\varepsilon_{\mathrm{ex}})/\partial N$. As mentioned in the text, the use of infinite square well wave functions is an approximation which destroys complete self-consistency of the 2D thickened Hartree-Fock results. The near unit overlap ($>98\%$) of the calculated Hartree wave function $\phi(z)$ with the simple square well result suggests the approximation is a good one. Figure 16 illustrates the substantial effect of this softening of the exchange energy on the compressibility parameter d_t. The horizontal dotted line is the noninteracting result $d_t=a_0/4$ valid in the ideally thin case while the solid curve adds in the exchange energy for this same ideal case [see Eq. (12)]. The dashed curve, however, includes the Coulomb softening, embodied in the form factor F, for 200-Å-wide quantum wells (but continues to omit the Hartree band-bending effects). Note that the first-order term in Eq. (A9) produces a uniform upward shift in the compressibility: $\Delta d_t/w\approx+0.050$.

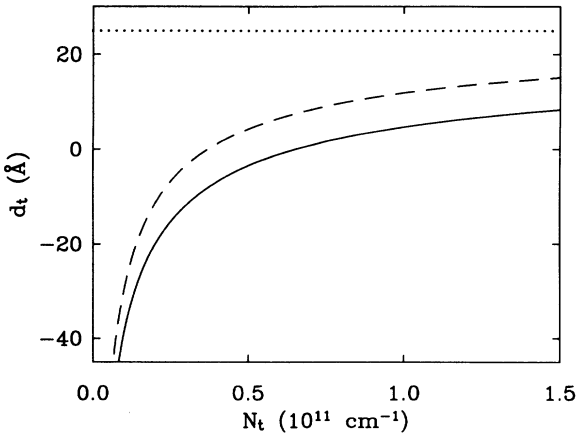

FIG. 16. Effect of exchange energy form factor on compressibility parameter d_t. Dotted line: Ideally thin 2DES, noninteracting. Solid line: Thin 2DES with simple exchange. Dashed line: "Thickened" exchange in 200-Å-wide quantum well. None of the curves contain the Hartree band-bending effect.

[1]For reviews of the FQHE, see *The Quantum Hall Effect,* edited by R. E. Prange and S. M. Girvin (Springer-Verlag, New York, 1987); also see T. Chakraborty and P. Pietilainen, in *The Fractional Quantum Hall Effect,* Springer Series in Solid-State Sciences Vol. 85 (Springer-Verlag, Berlin, 1988).

[2]D. C. Tsui, H. L. Stormer, and A. C. Gossard, Phys. Rev. Lett. **48**, 1559 (1982).

[3]E. Gornik *et al.*, Phys. Rev. Lett. **54**, 1820 (1985).

[4]J. K. Wang, J. H. Campbell, D. C. Tsui, and A. Y. Cho, Phys. Rev. B **38**, 6174 (1992).

[5]T. Haavasoja *et al.*, Surf. Sci. **142**, 294 (1984).

[6]J. P. Eisenstein *et al.*, Phys. Rev. Lett. **55**, 875 (1985).

[7]T. P. Smith, B. B. Goldberg, P. J. Stiles, and M. Heiblum, Phys. Rev. B **32**, 2696 (1985).

[8]V. Mosser, D. Weiss, K. v. Klitzing, K. Ploog, and G. Weimann, Solid State Commun. **58**, 5 (1986).

[9]R. C. Ashoori and R. H. Silsbee, Solid State Commun. **81**, 821 (1992).

[10]R. L. Willett, H. L. Stormer, D. C. Tsui, A. C. Gossard, and J. H. English, Phys. Rev. B **37**, 8476 (1988).

[11]There have been a great many calculations of the FQHE gap, see Ref. 1 for reviews.

[12]J. P. Eisenstein, L. N. Pfeiffer, and K. W. West, Phys. Rev. Lett. **68**, 674 (1992).

[13]See, A. L. Fetter and J. D. Walecka, *Quantum Theory of Many-Particle Systems* (McGraw-Hill, New York, 1971).

[14]T. P. Smith, W. I. Wang, and P. J. Stiles, Phys. Rev. B **34**, 2995 (1986); S. I. Dorozhkin, G. V. Kravchenko, R. I. Haug, K. von Klitzing, and K. Ploog, JETP Lett. **58**, 834 (1993).

[15]For an early discussion see M. S. Bello, E. I. Levin, B. I. Shklovskii, and A. L. Efros, Zh. Eksp. Teor. Fiz. **80**, 1596 (1981) [Sov. Phys. JETP **53**, 822 (1981)].

[16]A. L. Efros, Solid State Commun. **65**, 1281 (1988); in *Proceedings of the International Conference on the Physics of Semiconductors,* edited by E. M. Anastassakis and J. D. Joannopoulos (World Scientific, Singapore, 1990), p. 59.

[17]S. V. Kravchenko, D. A. Rinberg, S. G. Semenchinsky, and V. M. Pudalov, Phys. Rev. B **42**, 3741 (1990); S. V. Kravchenko, V. M. Pudalov, and S. G. Semenchinsky, Phys. Lett. **141**, 71 (1989); S. V. Kravchenko, J. M. Caulfield, J. Singleton, Hans Nielsen, and V. M. Pudalov, Phys. Rev. B **47**, 12 961 (1993).

[18]J. P. Eisenstein, in *Low Dimensional Systems: New Concepts,* edited by G. Bauer, F. Kuchar, and H. Heinrich, Springer Series in Solid State Sciences Vol. 111 (Springer-Verlag, Berlin, 1992), p. 167.

[19]J. N. Zemel and M. Kaplit, Surf. Sci. **13**, 17 (1969).

[20]Lian Zheng and A. H. MacDonald, Phys. Rev. B **49**, 5522 (1994).

[21]Serge Luryi, Appl. Phys. Lett. **52**, 501 (1988).

[22]L. N. Pfeiffer, E. F. Schubert, K. W. West, and C. Magee, Appl. Phys. Lett. **58**, 2258 (1991).

[23]J. P. Eisenstein, L. N. Pfeiffer, and K. W. West, Appl. Phys. Lett. **57**, 2324 (1990).

[24]S. Adachi, J. Appl. Phys. **58**, R1 (1985).

[25]S. Nagano, K. S. Singwi, and S. Ohnishi, Phys. Rev. B **29**, 1209 (1984).

[26]P. P. Ruden and Z. Wu, Appl. Phys. Lett. **59**, 2165 (1991). See also Y. Katayama, D. C. Tsui, H. C. Manoharan, and M.

Shayegan, Surf. Sci. **305**, 405 (1994). A. H. MacDonald (private communication) has suggested, however, that a transition to a bilayer state with spontaneous interlayer quantum coherence might occur and eliminate the exchange-driven instability.

[27]B. Tanatar and D. M. Ceperley, Phys. Rev. B **39**, 5005 (1989).

[28]Frank Stern, Jpn. J. Appl. Phys. Suppl. **2**, 323 (1974).

[29]P. J. Price, Phys. Rev. B **30**, 2234 (1984).

[30]We learned recently of compressibility calculations by A. Gold and L. Calmels [Solid State Commun. **88**, 659 (1993)]. While the Coulomb softening due to finite quantum well thickness is included, the Hartree band-bending effect is not.

[31]J. Hu and A. H. MacDonald provided us with the results of some initial calculations.

[32]Our numerical work has shown that it is possible, with good accuracy, to separate the various contributions (kinetic, Hartree, and electron-electron interaction) to the net $\partial\mu/\partial N$. For the Hartree piece we find $d_t(\text{Å}) \approx [-23.9+3.2\times N_t(10^{11}\ \text{cm}^{-2})]$. This formula is valid at both zero and high magnetic field, provided the in-plane dynamics are decoupled from the z motion.

[33]Frank Stern and Sankar Das Sarma, Phys. Rev. B **30**, 840 (1984).

[34]L. Hedin and B. I. Lundqvist, J. Phys. C **4**, 2064 (1971).

[35]For a discussion of the thermodynamics of the interacting 2DES at high magnetic fields, see A. H. MacDonald, H. C. A. Oji, and K. L. Liu, Phys. Rev. B **34**, 2681 (1986).

[36]D. Levesque, J. J. Weis, and A. H. MacDonald, Phys. Rev. B **30**, 1056 (1984).

[37]Lynn Bonsall and A. A. Maradudin, Phys. Rev. B **15**, 1959 (1977).

[38]G. Fano and F. Ortolani, Phys. Rev. B **37**, 8179 (1988).

[39]B. I. Halperin, P. A. Lee, and N. Read, Phys. Rev. B **47**, 7312 (1993).

[40]J. K. Jain, Phys. Rev. Lett. **63**, 199 (1989).

[41]F. G. Pikus and A. L. Efros, Phys. Rev. B **47**, 16 395 (1993).

[42]A. H. MacDonald, K. L. Liu, S. M. Girvin, and P. M. Platzman, Phys. Rev. B **33**, 4014 (1986).

[43]J. P. Eisenstein, L. N. Pfeiffer, and K. W. West, Phys. Rev. Lett. **69**, 3804 (1992); Surf. Sci. **305**, 393 (1994).

[44]In a recent tunneling experiment Boebinger *et al.* [Phys. Rev. B **47**, 16 608 (1993)] presented data showing a chemical potential jump at $\nu=\frac{1}{3}$ at $B=35$ T.

[45]A. H. MacDonald (unpublished).

[46]A. H. MacDonald and S. M. Girvin, Phys. Rev. B **34**, 5639 (1986).

[47]A. H. MacDonald (private communication).

[48]D. Yoshioka, J. Phys. Soc. Jpn. **55**, 885 (1985).

[49]For an early example see G. S. Boebinger *et al.*, Phys. Rev. B **36**, 7919 (1987).

[50]S. Q. Murphy, J. P. Eisenstein, L. N. Pfeiffer, and K. W. West, Bull. Am. Phys. Soc. **38**, 591 (1993); see also J. P. Eisenstein, L. N. Pfeiffer, and K. W. West, Appl. Plys. Lett. **58**, 1497 (1991).

[51]Noam Sivan, Phys. Rev. B **42**, 3183 (1990).

[52]J. P. Eisenstein and A. H. MacDonald (unpublished).

[53]C. Gros and A. H. MacDonald, Phys. Rev. B **42**, 9514 (1990), but see also Ref. 39.

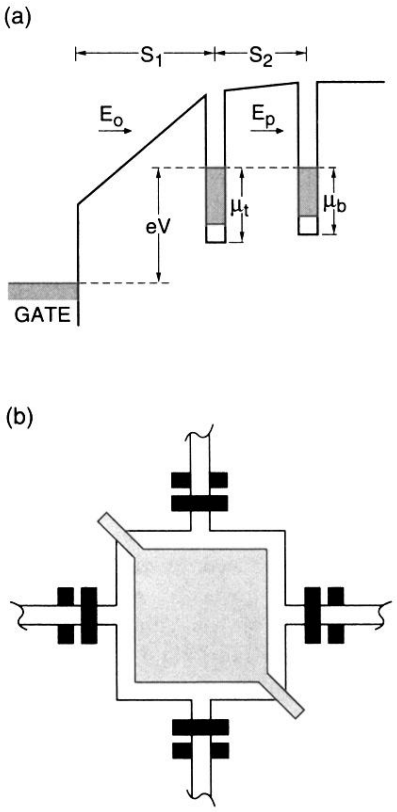

FIG. 2. (a) Simplified band diagram of the gated double quantum well structure. The shaded region in each quantum well denotes the Fermi distribution of the 2D electrons. The chemical potentials $\mu_{t,b}$ are measured relative to the bottoms of the individual wells. (b) Mesa and gate layout. The central mesa and gate squares are 250 and 210 μm, respectively, on a side. Each of the mesa arms is terminated with an indium Ohmic contact and has two associated gates, on the sample front and back sides, used for establishing separate connections to the individual 2D electron layers.